Characterization of Non-Traditional Loading of Piezoelectric Compliant Layer Adaptive Composite Stacks

By
Luke Lindemann
B.Sc., University of Kansas, Lawrence, 2019

Submitted to the graduate degree program in Mechanical Engineering and the Graduate Faculty of the University of Kansas in partial fulfillment of the requirements for the degree of Master of Science.

Chair: Lisa Friis, PhD

Carl Luchies, PhD

Gibum Kwon, PhD

Date Defended: 3 September 2021

The thesis committee for Luke Lindemann certifies that this is the approved version of the following thesis:

Characterization of Non-Traditional Loading of Piezoelectric Compliant Layer Adaptive Composite Stacks

Chairperson: Lisa Friis, PhD

Date Approved: 3 September 2021

Abstract

The overall goal of this study was to characterize piezoelectric materials in terms of non-traditional loading, namely tension and ultrasound loading. Compliant Layer Adaptive Composite Stacks (CLACS) consisting of 5 lead zirconate titanate (PZT) disks separated by composite layers were used throughout. Each disk was poled radially (R) or through (T) thickness, to create three types of CLACS: radial-poled (R), through-poled (T), and radial-through-poled (RT) CLACS. CLACS have been designed to harvest maximum power generation at low frequencies of loading. These systems allow for piezoelectric materials to use natural body loading, such as walking, to generate power for bone and soft tissue healing. Compression loading is the most common technique for producing power generation from piezoelectric materials, but in the present study, tension and ultrasound were tested as unconventional modes of loading. In contrast to compression loading, tension loading exhibited little power generation at low frequencies. Tension does not appear to markedly alter the power generated by compression loads, as there was not a significant difference in the power generated by compression before and after tension loading of the T-CLACS and RT-CLACS. However, the R-CLACS under a compression amplitude of 1000N produced statistically significant less power generation than after tension loading. The second unconventional mode of loading examined was ultrasound at the 0° orientation relative to the medial axis of the CLACS. Intensities of $0.5\ \mathrm{W/cm^2}$ and $1\ \mathrm{W/cm^2}$ produced power generation between 55 µW to 167 µW. This indicates that ultrasound probably has the capability to enhance bone and soft tissue healing, although ultrasound has a large mean coefficient of variation (66%). Thus, in conclusion, both unconventional loading methods used in this study, namely tension and ultrasound, tend to produce an increase in power generation, however the magnitude of the increase is much less

than that observed by compression loading. Overall, this study increases our understanding of the effects of tension and ultrasound on piezoelectric materials.

Acknowledgments

Dr. Elizabeth Friis

I would like to thank Dr. Friis for creating the positive learning environment in the lab. Thank you for leading me through research.

Dr. Kwon and Dr. Luchies

I would like to thank Dr. Kwon and Dr. Luchies for joining my committee. Over the years, I have learned many things from both of you, inside the classroom and out.

Dr. Linda D'Silva

I would like to thank Dr. D'Silva for letting me borrow the ultrasound machine within the chaos of COVID-19. Thank you for your support, and I wouldn't be able to finish without your help.

My lab mates at the university of Kansas

I would like to thank my lab mates Morghan Alters, Ryan Downing, Tori Drapal, Jordan Gamble, Evan Haas, Josh Koski, Dr. Ember Krech, Savanah Mosier, Anna Norman, Morgan Riley, and Chris Tacca for being open to questions about research. I am very thankful to have such a great group of friends under the same amount of stress.

My Family

I would like to thank my family for making me into the man I am today. Thank you all for supporting me through college and teaching me how to persevere. Special thanks to my grandfather, Dr. Curtis D. Klaassen, for teaching me how to write in a scientific manner.

Emmile Lindemann

I would like to thank my wife, Emmile, who is always there for me. I cherish the times that we have spent learning and growing together. Thank you for loving me well and supporting me during the hard and the good times.

Table of Contents

List of Figures

List of Tables

Chapter 1: Introduction

The average American breaks two bones in their lifetime. Failure of bone fractures to heal occurs in 5% to 10% of all patients, leading to non-unions. The FDA (Food and Drug Administration) categorizes a non-union as a bone fracture that has not healed for nine months and has shown no sign of healing for at least 3 months. For healthy bone growth, four factors need to be fulfilled. These factors include cellular environment, growth factors, bone matrix, and mechanical stability. If any of these four factors are not fulfilled, the break is predisposed to non-union (Calori et al., 2017). Non-unions especially affect those with comorbidities such as diabetes, using tobacco products, and osteoporosis. Diabetes and smoking increase the likelihood of infection at the fracture site by reducing growth factors and quality of the cellular environment (Marin et al., 2018; Sheung-tung, 2017). As of 2018, the CDC (Center of Disease Control and Prevention) estimated that ~8.5% of the US population has been diagnosed with diabetes and ~11.5% of the population uses tobacco products. Osteoporosis causes a decrease in bone density affecting the bone matrix and stability. Approximately 50% of women and 25% of men are affected by osteoporosis (Loi et al., 2016).

One common method of preventing non-union fractures is by internal fixation and electrical stimulation. This process has been utilized to aid in the prevention of non-unions and increasing the efficiency of bone growth (Griffin & Bayat, 2011). Piezoelectric materials possess the capability to convert mechanical strain into electrical energy. Piezoelectric materials have been shown to produce more electrical power when engineered into compliant layers, known as Compliant Layer Adaptive Composite Stacks (CLACS), rather than the traditional solid element.

Piezoelectric materials are usually compared by determining the power generated by compression. However, this study will focus on characterizing non-traditional loading on CLACS. The non-traditional loading conditions will be tension and ultrasound. Tension is present at natural loading of implants within the human body; therefore, it is important to understand how tension affects the CLACS system. Ultrasound might be useful to generate power from the CLACS when a patient is bedridden.

Chapter 2: Background

Process of Bone Remodeling

The human skeletal system is made up of all different types of bones for diverse purposes. Bone is used for protection, hearing, food digestion, and most commonly for body structure. Bones are all made up of the same basic components: calcium, phosphate, and collagen. These components form hard complex structures that allow bone to dynamically load and unload. Bone is constantly restructuring through osteoclasts and osteoblasts to strengthen the structure for different loading environments. This process, known as Wolff's Law, enables one to physically alter bone structure in a predictable way. Wolf's law is a mathematical model that shows how the internal structure will form over time due to introduced loads. Wolff's law is commonly misunderstood as the only mechanism responsible for altering bone structure, when in reality, there are more influences such as biological factors. However, Wolff's law does indicate that mechanical loading of bone plays a vital role in developing its structure (Ruff et al., 2006).

When bone is under load, mechano-transduction takes place. Mechano-transduction is when physical forces are converted into biological signals causing a cellular response. These signals are understood by the cells to remodel bone. This is especially present during bone fractures. In addition to biological signals, mechano-transduction also creates small electrochemical signals (Huang & Ogawa, 2010). It has been shown that bone cells have natural piezoelectric responses to mechanical loads. Bone cells can polarize themselves during cyclical mechanical stimuli, in turn changing their membrane potential. This change in potential affects how signaling pathways in the extracellular matrix operate. The change in signaling pathways regulates bone growth (Salter et al., 1997).

Fukada and Yasuda discovered in the 1950's a change in electrical potential via mechanically loading dry bone under compression. It was during this discovery that bone was shown to have piezoelectric properties. Dried bones were tested before and after boiling the bones, with no statistical difference in the piezoelectric constant, indicating there are non-biological reasons that the electrical potential was altered. The origin of the piezoelectric effect of the dried bone is ascribed to the crystalline micelle molecules within collagen. Human bone consists of collagen fibers that align with the length of the bone (ie. collagen fibrils align in a femur distally from the hip). As shown below, these crystalline micelle molecules align with the normal mechanical loading of the bone, creating a difference in electric potential (Fukada & Yasuda, 1957).

The electrical potential of bone under compression (blue arrows). Bending within the femur creates a side of tension that is positively charged (red plus symbols), and a side of compression that is negatively charged (red minus symbols).

Problems with Bone Fracture

The average American will break two bones within their lifetime. Failure of these fractures to heal occurs in 5% to 10% of all patients. When a fracture fails to heal, it is called a non-union (Zura et al., 2016). The FDA (Food and Drug Administration) categorizes non-union as a bone fracture that has not healed for 9 months and has shown no sign of healing for at least 3 months. For healthy bone growth, four factors need to be fulfilled. The factors include cellular environment, growth factors, bone matrix, and mechanical stability. If any of these four factors are not fulfilled, the break is predisposed to non-union (Calori et al., 2017). The cellular environment of the fracture must be able to sustain the growth of bone cells. It has been shown that comorbidities, such as diabetes and smoking, can increase the likelihood of infection. This can be detrimental to the healing of bone because a biofilm can form on the fracture site, stopping the development of osteoblasts and osteoclasts. These same comorbidities can result in decreased production of growth factors vital to the communication and growth of bone cells (Marin et al., 2018; Sheung-tung, 2017). The bone matrix is mostly affected by a decrease in bone density, also known as osteoporosis. Osteoporosis affects 50% of women, and 25% of men, showing this is one of the most common factors affecting bone growth (Loi et al., 2016). When faced with an unstable fracture, physicians primarily fixate the fracture using implants. This creates more mechanical stability to increase the likelihood the fracture will heal (Holmes, 2017). Non-unions often necessitate surgery, increasing pain, time, money, and in extreme cases the loss of limbs.

Electrical Stimulation

Electrical stimulation is one of the most common treatments to prevent and heal non-union fractures. Currently, there are three types of electrical stimulation approaches being used:

direct current (DC), capacitive coupling (CC), and inductive coupling (IC). DC stimulation is when a negative electrode is placed within the site of the break, creating a negative electric field. CC is noninvasively placing two electrodes on opposite sides of the bone, creating an electric field around the fracture site. The IC approach noninvasively places two copper coils close to the fracture site, creating an electric field. All use the same mechanism of creating an electrically negative field at the fracture site to promote bone growth (Griffin & Bayat, 2011). Although CC and IC are noninvasive techniques, they require a large amount of service. The patient must be compliant with wearing the device for long periods of time while keeping the device charged (Cottrill et al., 2019).

One of the main problems with DC stimulation is that it requires a second surgery to retrieve the device after the battery is depleted. This can cause prolonged pain and increase the risk of secondary infection (Brighton et al., 1981). One way that has been proposed to solve this problem is to embed a piezoelectric material into the structure of an implant. The piezoelectric implant produces a negative field around the fracture site by the natural loading of the patient. The piezoelectric implant acts as a battery and does not need to be removed (Cadel et al., 2018).

Changing the electrical potential artificially can positively affect bone growth. As early as the 1980's researchers showed at low amperage, bone grew more rapidly than a non-charged fracture. In these studies, negative electrical potential from an outside power source was used to accelerate growth of bone (Baranowski et al., 1983). However, when a similar piezoelectric material was placed directly in the bone of chickens, the results were inconclusive as both the negative and positive poles affected bone formation (Schumacher et al., 1983). It was later shown that lead-zirconate-titanate (PZT) could produce adequate power generation for human loading (Cochran et al., 1985).

Piezoelectricity

Electrical charge produced by mechanical stress on a material is called piezoelectricity. First discovered by Jacques and Pierre Currie in 1880, it was noted that specific crystalline materials had electrical charge when put under tension or compression. It was later discovered that within the crystalline structure of the material, the grains form a dipole when introduced to certain temperatures or electromagnetic fields. These grains can be oriented along the electromagnetic field and fixed in place, creating remanent polarization. If stress is introduced in parallel to the remanent polarization, the power voltage output of the material will be higher than without polarization (APC International, 2011).

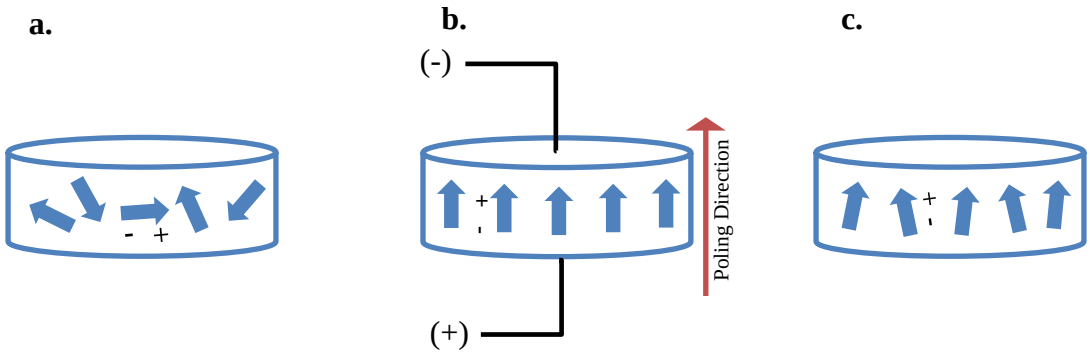

Poling direction of a piezoelectric material a) before, b) during, c) after the poling process.

The type of loading will determine the direction of the current produced by the material. For example, under tension, the poling direction will be positive to negative, while in compression the poling direction will be negative to positive, as shown below. The magnitude of power output is proportionate to the force applied. If the material is under electrical load, then the material will shrink or expand depending on the direction of the current. This is commonly seen with the use of ultrasound machines, where an AC current is introduced to a piezoelectric material producing ultrasonic waves (APC International, 2011; Carter & Kensley).

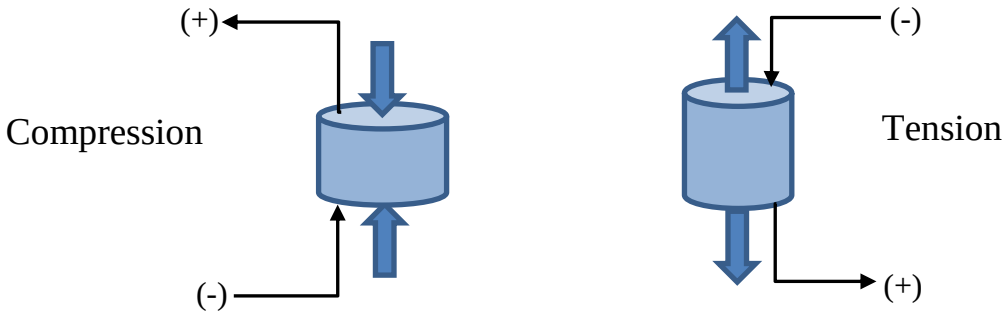

A piezoelectric material changing in polarity via compression (left) and tension (right) loading. The blue arrows represent the force on the piezoelectric material. The black arrows, plus and minus sign represent the flow of current.

Piezoelectric Materials

Today, we know of many piezoelectric materials such as quartz, zinc oxide, barium titanate (BaTiO3), and lead-zirconate-titanate (PZT). Most piezoelectric materials used in industry are ceramics, making them brittle in nature. The highest power density materials are synthetic ceramic materials (Guerin et al., 2019). These materials all have benefits, but the one chosen for this study was PZT due to its relatively high strength and low cost. PZT also has a high volume to power output, allowing it to be a prime material when space is restricted, like for the use of implants (Zhang et al., 2007).

Piezoelectric materials tend to produce higher electrical power with high frequency and high load applications. This is due to their high voltage, low current, and high impedance characteristics (Platt et al., 2005). The development of low-frequency energy harvesting with piezoelectric materials is a growing field. The opportunities to use these materials for power generation are immense. For example, there have been proposals to build sidewalks, bridges, shoes, and structures, as well as to harvest energy from ocean waves with piezoelectric materials

due to their ability to generate power. Within the human body, there are many different loading factors, compression, tension, bending, and torsion. All these loading conditions are experienced at natural frequencies and loading in the body. Platt et al. have shown ways of harvesting power from PZT materials at low frequencies. They placed PZT disks were placed in series and subjected to a compressive load parallel to the poling direction. This allowed for a decrease in impedance and an increase in effective capacitance, creating higher efficiency of power output, compared to a monolithic PZT column of the same volume (Platt et al., 2005).

To further improve the output of piezoelectric materials for low-frequency power generation, compliant layers were added to the stack system described by Platt et al. The addition of compliance layers significantly increased the power output of a stack with the same volume of PZT material (Krech et al., 2018). Krech called these devices CLACS. The addition of compliant layers also greatly increased the toughness of the material, making it more suitable for implant applications (Krech et al., 2018). In a finite element analysis (FEA) simulation of a CLACS system, the PZT disks had higher radial and Z-strain when epoxy encapsulation thickness was increased (Cadel et al., 2018). Cadel also reported higher effective strain when epoxy compliant layer thickness increases. When effective strain increases, the potential to produce electricity from PZT also increases (Cadel et al., 2018).

Forms of Loading

Traditionally piezoelectric materials are designed for compression due to their brittle nature. As the potential for power generation of a piezoelectric material increases, they become more brittle (Cain et al., 1999). This causes problems for the material to be placed under loading other than compression, due to their inability to yield. While compression is one of the most common loading conditions found in the body, there are other forces that are within this

environment creating multiaxial loads. These forces will be present within skeletal implants, making it highly important to understand how CLACS react in these environments.

Natural loading on the skeletal system involves both frequency and force. As a human moves, bones are placed under stress from impacts and muscle contraction. As a human walks, the legs and spine experience load at a low frequency matching the person's pace. While most bones are under compression, they also experience bending. Bending causes a side of compression and a side of tension. The highest tension found in the body while walking is through bending from the femur. The femoral head is slightly out of plane with the normal loading axis starting between the femoral condyles. This causes bending, creating a side of tension reaching 1.5 body weight during walking (Duda et al., 1997). Tension is also found at different magnitudes during various movements.

Ultrasound

Ultrasound has been used for medical purposes for decades. The practice has been shown to be helpful for both imaging and therapeutic applications. Ultrasound machines work by alternating current on a piezoelectric crystal, producing a high-frequency wave that travels through tissue. The crystal expands and contracts depending on the polarity of the electrical charge, creating ultrasonic waves. As seen below, the material properties of the medium cause the waves to attenuate, scatter, reflect, or absorb (Falyar, 2017). Attenuation (a) is the weakening of the sound wave through the medium, limiting the distance a wave can travel. Reflection (c) happens when waves bounce off a surface and disperse wave energy either directly back to the transducer or nonparallel to the wave pattern. Similarly, scattering (b) causes waves to be reflected, but in all directions, depending on the frequency and intensity of the waves, the

attenuation is affected. Absorption (d) is the energy of the wave being absorbed by the medium, dissipating as heat energy (Shriki, 2014).

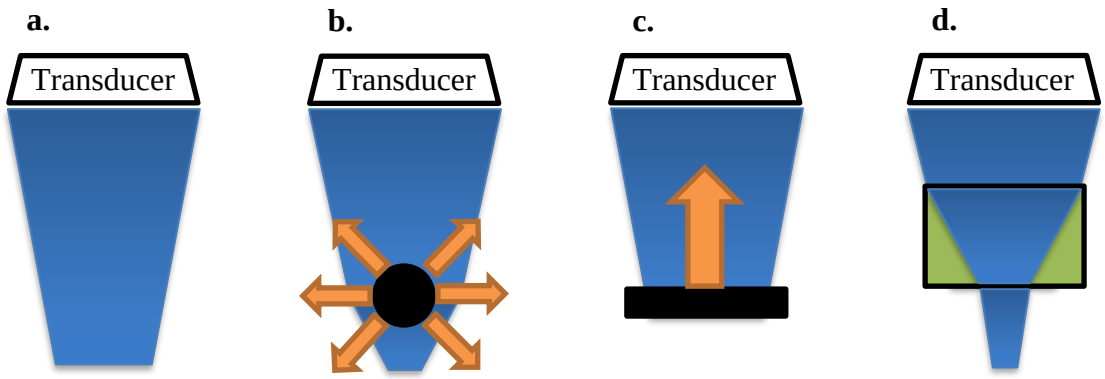

Depending on the material properties ultrasound waves travel through, the wave energy can a) attenuate, b) scatter, c) reflect, or d) absorb.

An ultrasound wave is classified as a soundwave ranging from 20kHz to 20MHz, well above the frequency a human ear can register. With each wave, a certain amount of mechanical energy is released, referred to as intensity. Specifically, intensity is the measure of the concentration of energy in the cross-section of a sound wave, often quantified as W/cm^2. Both frequency and intensity are needed to control ultrasonic waves for the purpose of imaging and therapy (Leighton, 2007). Frequencies between 1MHz to 20MHz and intensities ranging from 0.05-0.5W/cm^2 are used to create images for diagnoses. These images can depict almost every tissue in the human body, including fluid flow when dye is used. Higher frequencies can create a sharper image but will not reach deep tissues (Xin et al., 2016).

Therapeutic ultrasound utilizes the mechanical motion of waves to physically interact with tissue. This use of ultrasound has been shown to help with drug delivery, dissolve blood clots, heat tissue, and tissue ablation (Tsaklis, 2010). Therapeutic ultrasound requires higher intensity and lower frequencies than ultrasound imaging. This allows for larger amounts of

energies to penetrate the tissue, reaching a focal point. The focal point can change due to the acoustic properties of the tissue, as well as intensity and frequency. This is all considered while using both forms of ultrasound techniques. Two forms of ultrasound therapy are thermal and non-thermal. The thermal energy of the mechanical waves can be concentrated into a point creating a hot spot. Once a portion of tissue is warmed, the body increases blood flow to that area. This hot spot can be useful for several different procedures including reductions in joint stiffness and muscle spasm (Ogden et al., 2001). Non-thermal energy of the wave can vibrate small air bubbles in the tissue called cavitation. Vibrating cavitation bubbles can create stress to the surrounding cells within the tissue. This can aid in drug delivery and tissue ablation (Kooiman et al., 2020). In theory, ultrasound waves have the mechanical energy to excite piezoelectric materials to create electricity. Alters et al. have shown that an ultrasound transducer 20mm away form a PZT disk will produce power, although it had a high coefficient of variance (Alters, 2019). Utilizing ultrasound to produce electricity within an implant, could aid in helping bedridden patients

Degradation

Piezoelectric materials can both degrade and fatigue due to the environment. Over time poling direction can become disordered, lowering the effectiveness of the material to produce electricity (Lowrie, 1999). The material can also be stressed, creating microfractures within the material. Platt et al. studied PZT under a 1Hz load of 440N, showing that over a span of 10,000 cycles, PZT showed little degradation. It was also shown that with a pause of 30 minutes, the material significantly recovered (Platt et al., 2005). Although very little work has been done on exploring PZT fatigue and degradation at low frequencies with high amplitude, Platt's study shows that PZT would be a viable material for implants because human loading is sporadic. With

the addition of compliant layers within the CLACS, the longevity of the PZT disks should also have less fatigue. This can be seen by the work of van den Ende et al. with a stack made from PZT, epoxy-based adhesive, and silicone-based adhesive to form an actuator. They recorded that the silicone-based adhesive prevented crack formation and propagation (van den Ende et al., 2009). While this was done for an actuator instead of a generator, the same material properties should be seen under both conditions. Currently, there is no known research showing the fatigue and degradation of untraditional loading on PZT.

Current Uses of CLACS

Using piezoelectric materials within implants has become more practical with recent advances within power generation techniques. A spinal interbody cage was made using layers of PZT fibers by Goetzinger et al. It was shown that with more layers of fibers, the cage would more efficiently produce electrical power (Goetzinger et al., 2016). Utilizing this design in a pilot study, Friis et al. implanted a powered and control spinal fusion devise in the spines of mature sheep. Results showed powered spinal fusion was superior to the control (Friis et al., 2015). The layering technique was later utilized by Krech et al. with the addition of epoxy-compliant layers. The addition of compliant layers significantly increased the power generation under compression (Krech et al., 2018). This method reduces the volume of the PZT needed, lowering cost, and further expanding the uses within implants. Compliant layers also increase the strength of the stack, not only for compression but all modes of loading. The present research will explore the non-traditional loading of the stack configuration of CLACS to further understand the implications of tension and ultrasound.

References

Alters, M. (2019). *Determination of clinical efficacy of ultrasound stimulation on piezoelectric composites for power generation applications* [Master's Thesis, University of Kansas]. ProQuest Dissertations Publishing.

APC International, L. (2011). *Piezoelectric Ceramics: Principles and Applications*. APC International. https://books.google.com/books?id=nUafpwAACAAJ

Baranowski, T. J., Black, J., Brighton, C. T., & Friedenberg, Z. B. (1983). Electrical osteogenesis by low direct current. *Journal of Orthopaedic research*, *1*(2), 120-128.

Brighton, C. T., Black, J., Friedenberg, Z., Esterhai, J., Day, L., & Connolly, J. (1981). A multicenter study of the treatment of non-union with constant direct current. *JBJS*, *63*(1), 2-13.

Cadel, E. S., Krech, E. D., Arnold, P. M., & Friis, E. A. (2018). Stacked PZT Discs Generate Necessary Power for Bone Healing through Electrical Stimulation in a Composite Spinal Fusion Implant. *Bioengineering*, *5*(4), 90.

Cain, M. S., M; Gee, MG. (1999). *Degradation of Piezoelectric Materials*.

Calori, G. M., Mazza, E. L., Mazzola, S., Colombo, A., Giardina, F., Romanò, F., & Colombo, M. (2017). Non-unions. *Clinical Cases in Mineral and Bone Metabolism*, *14*(2), 186.

Carter, R., & Kensley, R. Introduction to Piezoelectric Transducers. *Midé Technology Corp., Woburn, MA. Google Scholar*.

Cochran, G., Johnson, M., Kadaba, M., Vosburgh, F., Ferguson-Pell, M., & Palmeiri, V. (1985). Piezoelectric internal fixation devices: A new approach to electrical augmentation of osteogenesis. *Journal of Orthopaedic research*, *3*(4), 508-513.

Cottrill, E., Pennington, Z., Ahmed, A. K., Lubelski, D., Goodwin, M. L., Perdomo-Pantoja, A., Westbroek, E. M., Theodore, N., Witham, T., & Sciubba, D. (2019). The effect of electrical stimulation therapies on spinal fusion: a cross-disciplinary systematic review and meta-analysis of the preclinical and clinical data. *Journal of Neurosurgery: Spine*, *32*(1), 106-126.

Duda, G. N., Schneider, E., & Chao, E. Y. (1997). Internal forces and moments in the femur during walking. *J Biomech*, *30*(9), 933-941. https://doi.org/10.1016/s0021-9290(97)00057-2

Falyar, C. R. (2017). *Reflection, Refraction, Scattering, and Attenuation*. https://www.vaultrasound.com/educational-resources/ultrasound-physics/reflection-refraction/

Friis, E. A. G. S., Arnold PM. (2015). DC stimulation for spinal fusion with a piezoelectric composite material interbody implant: An ovine pilot study. *Society For Biomaterials*. (abstract)

Fukada, E., & Yasuda, I. (1957). On the Piezoelectric Effect of Bone. *Journal of the Physical Society of Japan*, *12*(10), 1158-1162. https://doi.org/10.1143/JPSJ.12.1158

Goetzinger, N. C., Tobaben, E. J., Domann, J. P., Arnold, P. M., & Friis, E. A. (2016). Composite piezoelectric spinal fusion implant: Effects of stacked generators. *J Biomed Mater Res B Appl Biomater*, *104*(1), 158-164. https://doi.org/10.1002/jbm.b.33365

Griffin, M., & Bayat, A. (2011). Electrical stimulation in bone healing: critical analysis by evaluating levels of evidence. *Eplasty*, *11*.

Guerin, S., Tofail, S. A., & Thompson, D. (2019). Organic piezoelectric materials: milestones and potential. *NPG Asia Materials*, *11*(1), 1-5.

Holmes, D. (2017). Non-union bone fracture: a quicker fix. *Nature*, *550*(7677), S193-S193.

Huang, C., & Ogawa, R. (2010). Mechanotransduction in bone repair and regeneration. *The FASEB Journal*, *24*(10), 3625-3632.

Kooiman, K., Roovers, S., Langeveld, S. A. G., Kleven, R. T., Dewitte, H., O'Reilly, M. A., Escoffre, J. M., Bouakaz, A., Verweij, M. D., Hynynen, K., Lentacker, I., Stride, E., & Holland, C. K. (2020).

Ultrasound-Responsive Cavitation Nuclei for Therapy and Drug Delivery. *Ultrasound Med Biol*, *46*(6), 1296-1325. https://doi.org/10.1016/j.ultrasmedbio.2020.01.002

Krech, E. D., Cadel, E. S., Barrett, R. M., & Friis, E. A. (2018). Effect of compliant layers within piezoelectric composites on power generation providing electrical stimulation in low frequency applications. *J Mech Behav Biomed Mater*, *88*, 340-345. https://doi.org/10.1016/j.jmbbm.2018.08.027

Leighton, T. G. (2007). What is ultrasound? *Progress in Biophysics and Molecular Biology*, *93*(1), 3-83. https://doi.org/https://doi.org/10.1016/j.pbiomolbio.2006.07.026

Loi, F., Córdova, L. A., Pajarinen, J., Lin, T.-h., Yao, Z., & Goodman, S. B. (2016). Inflammation, fracture and bone repair. *Bone*, *86*, 119-130.

Lowrie, F. C., MG; Stewart, M; Gee MG. (1999). *Time dependent behaviour of piezo-electric materials* [NPL Report]. http://eprintspublications.npl.co.uk/1059/

Marin, C., Luyten, F. P., Van der Schueren, B., Kerckhofs, G., & Vandamme, K. (2018). The impact of type 2 diabetes on bone fracture healing. *Frontiers in Endocrinology*, *9*, 6.

Ogden, J. A., Tóth-Kischkat, A., & Schultheiss, R. (2001). Principles of shock wave therapy. *Clin Orthop Relat Res*(387), 8-17. https://doi.org/10.1097/00003086-200106000-00003

Platt, S. R., Farritor, S., & Haider, H. (2005). On low-frequency electric power generation with PZT ceramics. *IEEE/ASME Transactions on Mechatronics*, *10*(2), 240-252. https://doi.org/10.1109/TMECH.2005.844704

Ruff, C., Holt, B., & Trinkaus, E. (2006). Who's afraid of the big bad Wolff?:"Wolff's law" and bone functional adaptation. *American Journal of Physical Anthropology: The Official Publication of the American Association of Physical Anthropologists*, *129*(4), 484-498.

Salter, D., Robb, J., & Wright, M. (1997). Electrophysiological responses of human bone cells to mechanical stimulation: evidence for specific integrin function in mechanotransduction. *Journal of Bone and Mineral Research*, *12*(7), 1133-1141.

Schumacher, D., Strunz, V., & Gross, U. (1983). Does piezoceramic influence avian bone formation in the early postoperative phase? *Biomaterials*, *4*(3), 215-217.

Sheung-tung, H. (2017). Quit Smoking before orthopeadic surgery. Journal of Orthopeadics, Trauma and Rehabilitation, A1-A3. https://doi.org/10.1016/j.jotr.2017.10.001

Shriki, J. (2014). Ultrasound physics. *Crit Care Clin*, *30*(1), 1-24, v. https://doi.org/10.1016/j.ccc.2013.08.004

Tsaklis, P. (2010). Presentation of acoustic waves propagation and their effects through human body tissues. *Human Movement*, *11*. https://doi.org/10.2478/v10038-009-0025-z

van den Ende, D., Bos, B., Groen, P., & Dortmans, L. M. J. G. (2009). Lifetime of piezoceramic multilayer actuators: Interplay of material properties and actuator design. *Journal of Electroceramics*, *22*, 163-170. https://doi.org/10.1007/s10832-007-9411-0

Xin, Z., Lin, G., Lei, H., Lue, T. F., & Guo, Y. (2016). Clinical applications of low-intensity pulsed ultrasound and its potential role in urology. *Transl Androl Urol*, *5*(2), 255-266. https://doi.org/10.21037/tau.2016.02.04

Zhang, S., Xia, R., & Shrout, T. R. (2007). Lead-free piezoelectric ceramics vs. PZT? *Journal of Electroceramics*, *19*(4), 251-257.

Zura, R., Xiong, Z., Einhorn, T., Watson, J. T., Ostrum, R. F., Prayson, M. J., Della Rocca, G. J., Mehta, S., McKinley, T., & Wang, Z. (2016). Epidemiology of fracture nonunion in 18 human bones. *JAMA surgery*, *151*(11), e162775-e162775.

Chapter 3: Manuscript in Preparation

This section contains a manuscript to be submitted for publication, some information is duplicated.

Characterization of Non-Traditional Loading of Piezoelectric Compliant Layer Adaptive Composite Stacks

Authors:
Luke Lindemann
Spine Biomechanics Laboratory
Department of Mechanical Engineering,
University of Kansas,
Lawrence, KS, 66045
Email: lindemannluke@gmail.edu

Elizabeth Friis *
Spine Biomechanics Laboratory
Department of Mechanical Engineering,
University of Kansas,
Lawrence, KS, 66045
Email: lfriis@ku.edu

* Corresponding Author

Abstract

The overall goal of this study was to characterize piezoelectric materials in terms of untraditional loading, such as tension and ultrasound loading. Compliant Layer Adaptive Composite Stacks (CLACS) consisting of 5 lead-zirconate-titanate (PZT) disks separated by composite layers were used throughout. Each disk was poled radially (R) or through (T) thickness, to create three types of CLACS: radial-poled (R), through-poled (T), and radial-through-poled (RT) CLACS. CLACS have been designed to harvest high power generation at low frequencies of loading. These systems allow for piezoelectric materials to use natural body loading, such as walking, to generate power for bone and soft tissue healing. Compression loading is the most common technique for producing power generation from piezoelectric materials, but in the present study, we examined tension and ultrasound as unconventional modes of loading. In contrast to compression loading, tension loading exhibited little power generation at low frequencies. Tension does not appear to markedly alter the power generated by compression loads, as in general there was not a significant difference in power generated by compression before and after tension loading of the T-CLACS and RT-CLACS. However, the R-CLACS under a compression amplitude of 1000N produced statistically significant less power generation than after tension loading. The second unconventional mode of loading examined was ultrasound at the 0° orientation relative to the medial axis of the CLACS. Intensities of $0.5\ \mathrm{W/cm^2}$ and $1\ \mathrm{W/cm^2}$ produced power generation between 55 µW to 167 µW. This indicates that ultrasound probably has the capability to enhance bone and soft tissue healing, although ultrasound has a high mean coefficient of variation (66%). Thus, in conclusion, both unconventional loading methods used in this study, namely tension and ultrasound, tend to produce an increase in power generation, however the magnitude of the increases is much less

than that observed by compression loading. Overall, this study increases our understanding of the effects of tension and ultrasound on piezoelectric materials.

Introduction

The average American breaks two bones in their lifetime. Failure of bone fractures to heal occurs in 5% to 10% of all patients, leading to non-unions. The FDA (Food and Drug Administration) categorizes a non-union as a bone fracture that has not healed for nine months and has shown no sign of healing for at least 3 months. For healthy bone growth, four factors need to be fulfilled. These factors include cellular environment, growth factors, bone matrix, and mechanical stability. If any of these four factors are not fulfilled, the break is predisposed to non-union (Calori et al., 2017). Non-unions especially affect those with comorbidities such as diabetes, using tobacco products, and osteoporosis. Diabetes and smoking increase the likelihood of infection at the fracture site by reducing growth factors and quality of the cellular environment (Marin et al., 2018; Sheung-tung, 2017). As of 2018, the CDC (Center of Disease Control and Prevention) estimated that ~8.5% of the US population has been diagnosed with diabetes and ~11.5% of the population uses tobacco products. Osteoporosis causes a decrease in bone density affecting the bone matrix and stability. Approximately 50% of women and 25% of men are affected by osteoporosis (Loi et al., 2016).

One common method of preventing non-union fractures is by internal fixation and electrical stimulation. When a bone is under load, it experiences a phenomenon called mechano-transduction. Mechano-transduction is when physical forces are converted into biochemical signals causing a cellular response. Some of those biochemical signals are the result of electrical charge produced by the bending of bone. Fukada and Yasuda discovered the piezoelectric

qualities of bone in 1957 (Fukada & Yasuda, 1957). This led to the understanding of the function of electrical charge in bone growth. When bone is in tension, a positive electrical field is observed that communicates to osteoclasts to remove bone structure. While bone is under compression, a negative electrical field is produced, communicating to the osteoblasts to build bone structure. This process has been utilized to aid in the prevention of non-unions and increasing the efficiency of bone growth (Griffin & Bayat, 2011).

Piezoelectric materials possess the capability to convert mechanical strain into electrical energy. Like bone, piezoelectric materials create an electrical charge under compression, tension, or bending. Traditionally, piezoelectric materials are utilized for compression due to their natural brittle properties. Lead-zirconate-titanate (PZT) is one of the more common piezoelectric materials that has high power output with low-frequency loading. Utilizing this material, a power generator can be designed to aid in the healing of bone. One issue that arises is the high impedance and low capacitance of piezoelectric materials, impeding power output. Platt et al. showed that by wiring PZT disks in series and mechanically loading the system in parallel, power could be more efficiently produced, due to the lowering of impedance (Platt et al., 2005).

Goetzinger et al. designed a spinal interbody cage, utilizing the layering method and PZT fibers, that produces an electrical field with natural loading from the body (Goetzinger et al., 2016). This devise was shown to improve spinal fusion in sheep (Friis et al., 2015). Electrical stimulation has also been utilized to promote soft tissue wound healing (Franklin et al., 2016). Krech et al. utilized the layering method with the addition of compliant layers and called the system CLACS. These compliant layers allowed the system to increase strength, making them more suitable for implants and non-traditional loading applications. The compliant layers also increased power output in compression (Cadel et al., 2018; Krech et al., 2018). The CLACS

system was also tested with PZT poled in different directions. The two poling directions of PZT were (1) from the center of the disk radially (R) and (2) through the thickness of the disks (T). Three different types of CLACS were made, the first type consisting of only radial-poled disks (R-CLACS), the second type with through-poled disks (T-CLACS), and the third type with both radially and through poled disks alternating in series (RT-CLACS).

This study will focus on characterizing non-traditional loading on the three CLACS. The non-traditional loading conditions will be tension and ultrasound. Tension is present at natural loading of implants within the human body; therefore, it is important to understand how tension affects the CLACS system. Ultrasound might be useful to generate power from the CLACS when a patient is bedridden.

Methods

Materials

Compliant layer adaptive composite stacks (CLACS) were created using five commercially available PZT-5A Navy Type II (SM412, STEMiNC, Doral, FL) disks wired in parallel using thin copper foil attached by conductive epoxy (EPO-TEK H20E, Epoxy Technology, Billerica, MA). A thinly sliced compliant layer was placed in-between each disk. The compliant layers had a thickness of 0.4 mm and a radius of 11mm, created from a column of EPO-TEK 301. The stack of PZT and epoxy was then placed into a mold of EPO-TEK epoxy creating a 11x150mm cylinder. On the top and bottom of the cylinder, tabs were formed for use as MTS grips. The inner stack was cured into place along the center axis of the cylinder, with lead wires protruding from the side.

The RT-CLACS were made from the same PZT material, disks were poled in either the radial direction or through direction. All PZT disks were poled by the manufacturer, STEMiNC (Davenport, FL). RT-CLACS have alternating through and radially poled PZT disks wired electrically in parallel.

Impedance and Capacitance

Each specimen's impedance and capacitance were recorded from a Hioki 3522-50 LCR HiTester (Hioki, Plano, TX). Impedance and capacitance values were collected at 3Hz and 5Hz, before and after each test to ensure the integrity of the piezoelectric stack. This information can also be used to help understand how the poling direction of the piezoelectric materials are reacting to different loading conditions.

Tension Loading

Three types of CLACS specimens, consisting of R-CLACS (N=4), T-CLACS (N=5), RT-CLACS (N=5) were placed into a bi-axial MTS MiniBionix 858 with 647 Hydraulic Wedge Grips (MTS, Eden Prairie, MN) one at a time. The specimens were aligned with the center axis of the hydraulic grips to ensure the force was parallel to the length of the specimen. A preload of 1200N was used with oscillating load amplitudes of 100N, 500N, and 1000N at frequencies of 0.5Hz, 1Hz, 2Hz, and 3Hz. A resistance box was in series to the specimen to control resistance sweep values ranging from 0MΩ to 20MΩ. The MTS DAQ system (MTS, Eden Prairie, MN) was used to record voltage output from the system over each loading condition. An analysis of variance test was used ($\alpha<0.05$) to compare the three types of CLACS poling direction.

Compression Loading

All CLACS were tested in compression before and after tension loading. Each specimen was placed under a preload of -1200N and load amplitudes of 100N, 500N, and 1000N at

frequencies of 3Hz and 5Hz. A resistance box was wired in series with the CLACS to control resistance sweep values ranging from 0.05 MΩ to 9 MΩ. The MTS DAQ system was used to record the voltage output with each load. An ANOVA test ($\alpha<0.05$) was used to compare compression tests before and after tension loading.

Ultrasound Loading

After both tension and compression loading was finished, the specimens were reshaped for ultrasound testing. The top and bottom of the specimen were cut to a manageable size, leaving 5 mm of the epoxy mold on one side. Once reshaped, the specimens were placed into a highly concentrated gelatin mixture within a mold made from a plexiglass box with one side consisting of a thin plastic film. The gelatin mixture acted as an ultrasound phantom, to help mimic the environment of an implant under soft tissue. The specimen was suspended 20 mm away from the thin plastic sheet, not touching any of the walls of the mold. An Intelect Transport 2-Channel Electrotherapy (Chattanooga Group, Dallas, TX) therapeutic ultrasound machine with a $5cm^2$ transducer face was used to generate the ultrasound waves. The transducer head of the ultrasound machine was covered in coupling gel and placed on the thin plastic film of the mold. Two different molds were created to allow for the transducer to be placed at 90° (side) and 0° (bottom) relative to the center medial line of the stack. The specimen was wired in series with a resistance box, and a TEKTRONIX Mixed Domain Oscilloscope (Beaverton, OR) with 2.5 GS/s sample rate, MDO3012. The ultrasound machine had a loading frequency of 1 MHz with intensities of $0.1\ \mathrm{W/cm^2}$, $0.5\ \mathrm{W/cm^2}$, and $1\ \mathrm{W/cm^2}$ at resistances between 0Ω and 350Ω. Between each data collection the CLACS were given 15 seconds to rest, and 15 seconds under ultrasound load to charge the material closer to its resonance frequency. The oscilloscope recorded voltage every 2μs for 2000 data points and was saved in a comma-separated values

(CSV) file type, during each loading condition. An ANOVA ($\alpha<0.05$) test was used to determine differences between specimen types.

Data Analysis

For all experiments, voltage data was collected and processed using MATLAB (MathWorks, Natick, MA) code. The raw voltage data obtained was imported into a MATLAB code that filtered the data and calculated the average maximum via the middle five cycles of voltage. The same code converted the average voltage amplitude to voltage root mean square (RMS):

$$(V_{RMS} = V_{amp}/\sqrt{2}).$$

Power was calculated for every loading condition:

$$(P = V_{RMS}^2/R)$$

Results

Effect of Tension

The effect of tension loading on power generation was recorded for radial-poled (R), through-poled (T), and radial-through-poled (RT) CLACS. A total of 14 CLACS were tested, four for R-CLACS, five for T-CLACS, and five for RT-CLACS. One R specimen was damaged and could not be used for MTS testing. No significant difference was seen in capacitance and impedance for the duration of the study, indicating the PZT disks were not damaged.

Figure 1 shows the effects of tension loading on power generation in CLACS for a single loading condition of 1000N and 3Hz, over resistance values from 80KΩ to 9MΩ. The highest efficiency of power generation was observed at approximately 2 MΩ for all three types of CLACS.

Figure 2 shows the effects of tension on power generation in radial-poled (R), through-poled (T), and radial-through-poled (RT) CLACS. The power generated by the CLACS was highly dependent on the loading conditions as seen in Figure 2 and Table 1. Tension amplitudes of 100N and 500N exhibited very low power generation. For example, tension amplitudes of 100N produced less than 0.66μW, and amplitudes of 500N produced between 2.3μW and 17μW of power. However, when the CLACS undergo a tension amplitude of 1000N, the power generated was between 10μW to 70μW.

Although there is no significant difference in power generation between the three types of CLACS, a trend of higher power generation was observed from the R-CLACS. For example, at loading conditions of 1000N and 3Hz, a 40% increase in power generation was observed from T-CLACS to R-CLACS, and a 20% increase from RT-CLACS to R-CLACS, however neither were statistically significant.

Table 2 indicates the coefficient of variation (CV) for power generation produced by the R-CLACS, T-CLACS, and RT-CLACS under various tension loads. The overall mean coefficient of variation for power generated by the three CLACS under various tensions was 38%, but the CV for T-CLACS was 61%, which is much higher than the approximate 26% CV observed for both the R-CLACS and RT-CLACS.

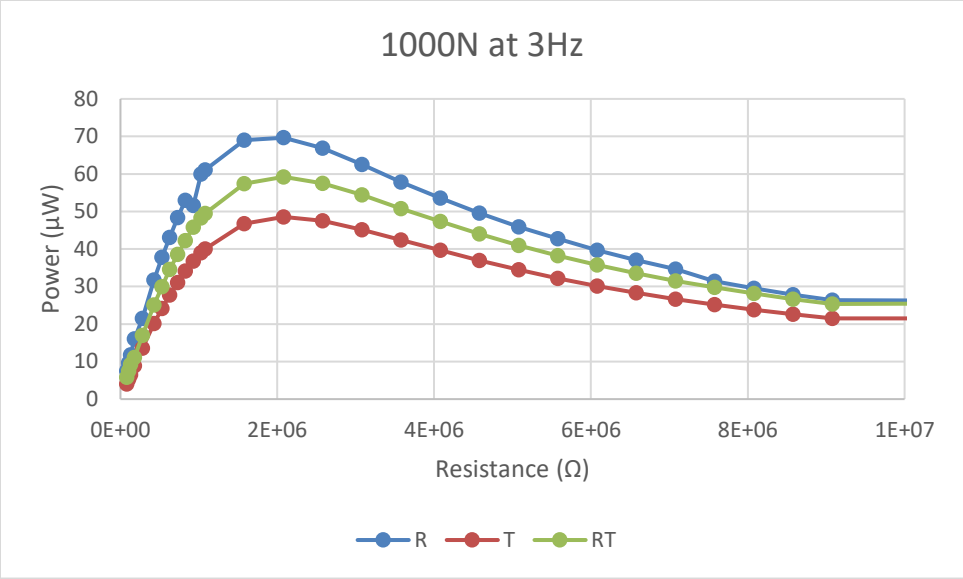

Figure 1: *Effect of tension on power generation on three types of CLACS: through-poled (T), radial-poled (R), and radial-through-poled (RT).*
This data was obtained using 1000N amplitude at 3Hz.

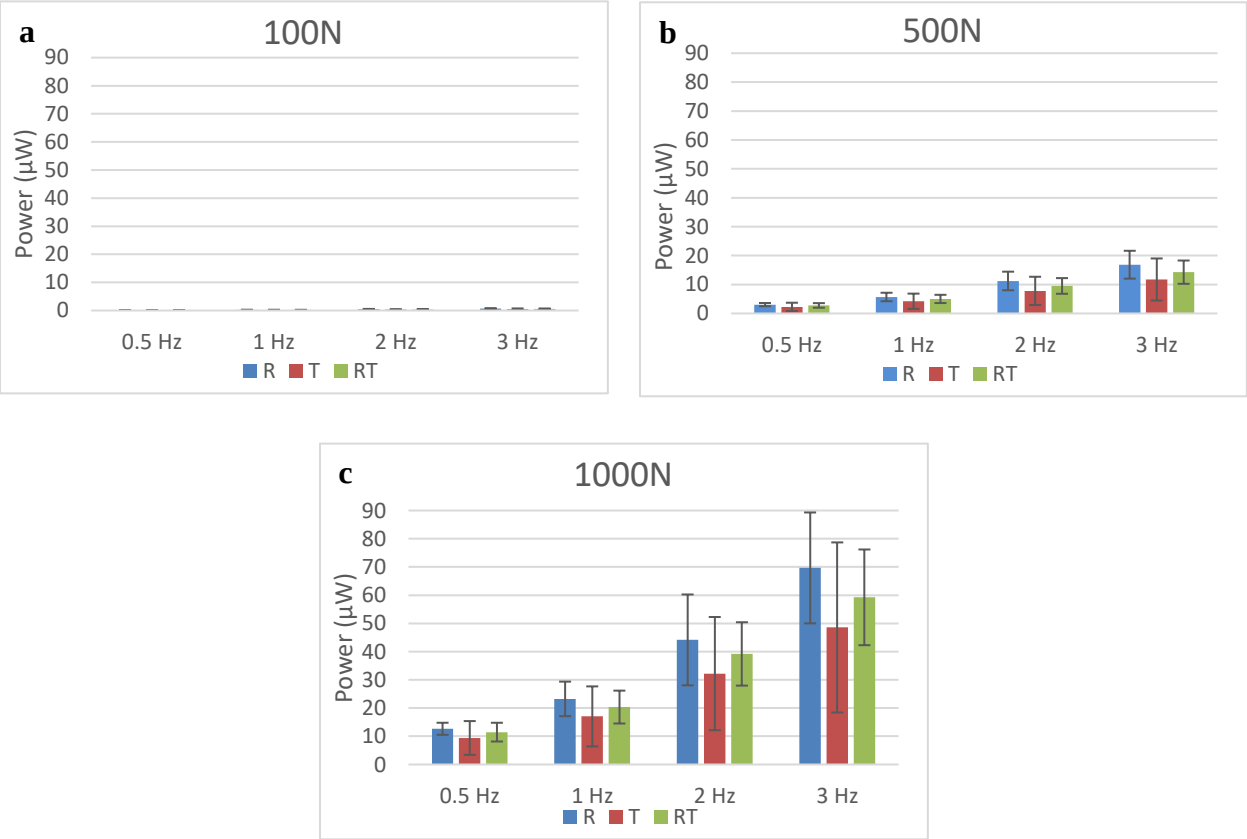

Figure 2: *Effect of tension on power generation of three types of CLACS: radial-poled (R), through-poled (T), and radial-through-poled (RT).*
Figure 2a, 2b, and 2c represent experiments at 100N, 500N, and 1000N amplitude, respectively. Power represents the maximum power generated for each specimen. Each bar represents the mean ± SD of 4-5 CLACS.

Table 1: *Effect of tension on power generation on three types of CLACS: radial-poled (R), through-poled (T), and radial-through-poled (RT).*

		R	T	RT
Frequency	**Amplitude**	**Power ± SD (μW)**	**Power ± SD (μW)**	**Power ± SD (μW)**
0.5 Hz	**100N**	0.12 ± 0.02	0.09 ± 0.05	0.11 ± 0.03
	500N	3.06 ± 0.56	2.27 ± 1.44	2.78 ± 0.79
	1000N	12.6 ± 2.14	9.39 ± 5.99	11.5 ± 3.32
1 Hz	**100N**	0.23 ± 0.06	0.17 ± 0.10	0.21 ± 0.05
	500N	5.69 ± 1.46	4.21 ± 2.65	5.02 ± 1.42
	1000N	23.3 ± 6.12	17.0 ± 10.6	20.4 ± 5.83
2 Hz	**100N**	0.44 ± 0.13	0.31 ± 0.18	0.39 ± 0.10
	500N	11.2 ± 3.22	7.81 ± 4.88	9.51 ± 2.70
	1000N	44.1 ± 16.1	32.2 ± 20.1	39.2 ± 11.2
3 Hz	**100N**	0.66 ± 0.19	0.46 ± 0.27	0.58 ± 0.14
	500N	16.9 ± 4.82	11.7 ± 7.27	14.3 ± 4.03
	1000N	69.7 ± 19.7	48.6 ± 30.1	59.2 ± 17.0

Table 2: *Effect of tension on the coefficient of variance (CV) for the three types of CLACS.*

Tension CV		**R (%)**	**T (%)**	**RT (%)**
Frequency	**Amplitude**			
0.5 Hz	**100N**	20.2	59.9	26.0
	500N	18.2	63.5	28.4
	1000N	17.0	63.8	29.0
1 Hz	**100N**	24.4	58.7	25.2
	500N	25.7	62.8	28.4
	1000N	26.3	62.5	28.6
2 Hz	**100N**	29.2	58.7	25.3
	500N	28.7	62.5	28.4
	1000N	36.5	62.3	28.7
3 Hz	**100N**	29.0	58.7	25.1
	500N	28.6	61.9	28.2
	1000N	28.2	62.1	28.6

Compression Loading

Figure 3 and Table 3 summarizes the effects of before and after tension on power generation via compression in radial-poled (R), through-poled (T), and radial-through-poled (RT) CLACS. The power generated by the CLACS was highly dependent on the loading conditions. For example, when the CLACS were tested at 500N and 3Hz, 500N and 5Hz, 1000N and 3Hz, as well as 1000N and 5Hz, approximately 78 to 102 μW, 131 to 171 μW, 306 to 421 μW, and 503 μW to 701 μW were generated, respectively.

The power generated by compression, after the tension experiment, tended to be lower than the power generated by compression before the tension experiment. R-CLACS under an amplitude load of 1000N at both 3Hz, produced approximately 70μW less power at post-tension compression loading than at pre-tension compression loading. While the compression power output after the tension experiment tended to be lower under all loading conditions, only the R-CLACS under an amplitude of 1000N at both 3Hz and 5Hz show statistically ($p<0.05$) significant lower power generation in the post-tension loading.

Table 4 shows the coefficient of variation of power generation by compression before and after tension loading. The pre-tension loading has a mean CV of 12%, while post-tension loading shows a mean of 14%, indicating relatively low variation and that tension loading has little effect on the CV. Less variance was observed with the R-CLACS (mean CV of 7%), verses a mean CV ranging from 12.5% to 18% in the T-CLACS and RT-CLACS in this experiment.

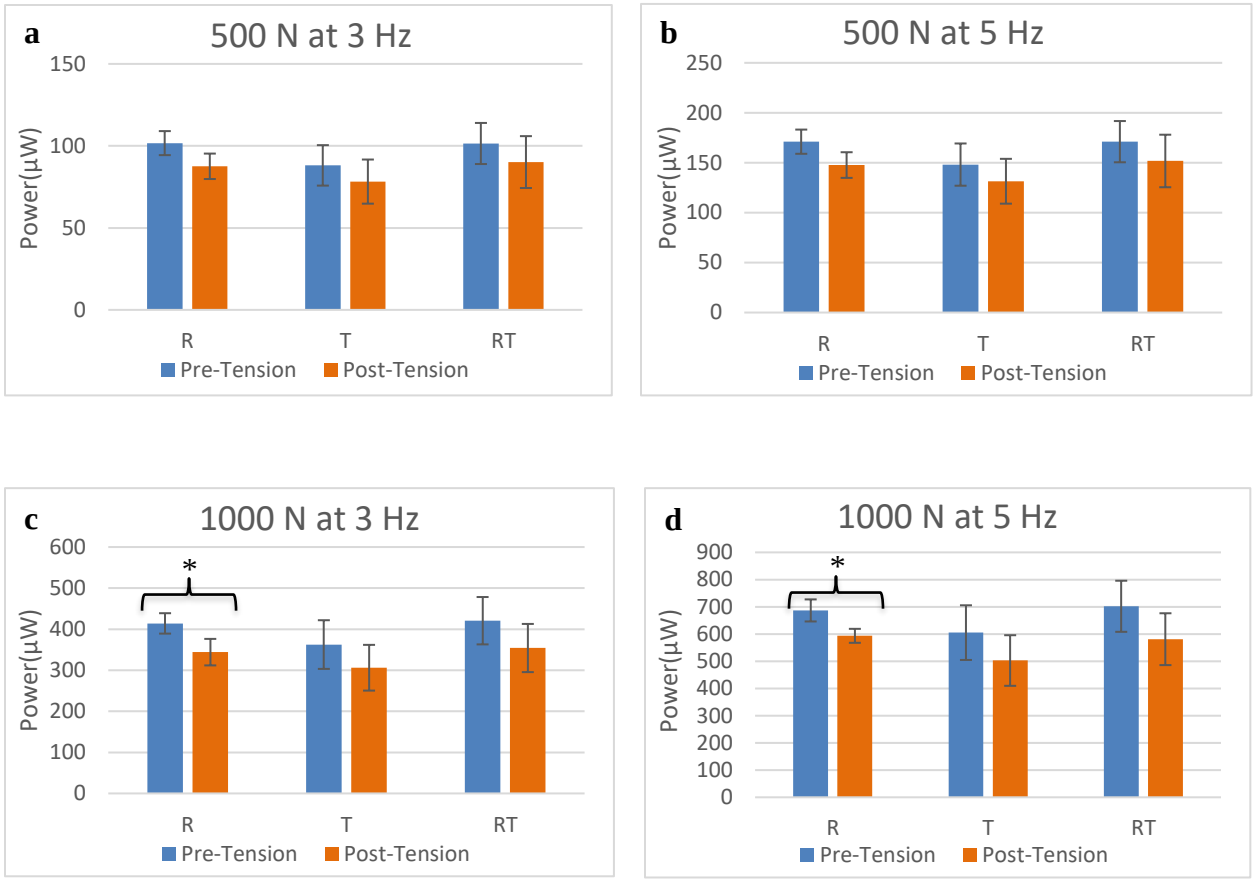

Figure 3: *Effect of before and after tension on power generation via compression loading on three types of CLACS: radial-poled (R), through-poled (T), and radial-through-poled (RT).*
Power represents the maximum power generated by each specimen. Blue bars represent power before tension, and orange bars after tension, including the SD of 4-5 CLACS. Asterisk represents statistical significance at $p<0.05$.

Table 3: *Effect of before and after tension on power generation via compression loading on three types of CLACS: radial-poled (R), through-poled (T), and radial-through-poled (RT). Asterisk represent statistically difference between pre- and post-tension (α<0.05).*

Load	Frequency	Pre-tension			Post-tension		
		R	T	RT	R	T	RT
500N	3 Hz	102 ± 7.3	88.1 ± 12.3	106 ± 12.6	87.6 ± 7.8	78.2 ± 13.5	90.1 ± 15.8
	5 Hz	171 ± 12.1	148 ± 21.1	178 ± 21.1	148 ± 12.8	131 ± 22.4	152 ± 26.3
1000N	3 Hz	414* ± 24.8	363 ± 59.3	439 ± 56.8	344 ± 32.3	306* ± 28.3	354 ± 58.7
	5 Hz	687* ± 40.5	605 ± 100.4	734 ± 93.6	593 ± 25.7	503* ± 93.0	581 ± 95.2

Table 4: *Effect of compression on the coefficient of variation (CV) for the three types of CLACS.*

		500N		1000N	
		3 Hz (%)	5 Hz (%)	3 Hz (%)	5 Hz (%)
Pre-Tension	R	7.20	7.08	6.00	5.90
	T	14.0	14.3	16.3	16.6
	RT	11.9	11.8	12.9	12.8
Post-Tension	R	8.85	8.69	9.38	4.32
	T	17.2	17.1	18.2	18.5
	RT	17.5	17.3	16.6	16.4

Tension vs Compression

The effect of compression or tension on power generation of the three types of CLACS is shown in Figure 4 and Table 5. As noted previously, there is no statistical difference in power generation produced by tension by the three types of CLACS. However, the power generated by tension at both the 500N and 1000N amplitude was much lower than the power generated by compression at 500N and 1000N. The power generated from the CLACS under tension were approximately 83% lower than the power generated under compression.

Tension loading (Table 6) resulted in a much higher coefficient of variation (CV) of power generated, ranging from 28% to 62%, than that observed during compression loading (9-18%). Regarding the three types of CLACS, the T-CLACS showed higher CV (62%) than the R-CLACS and RT-CLACS (28%), especially with tension loading.

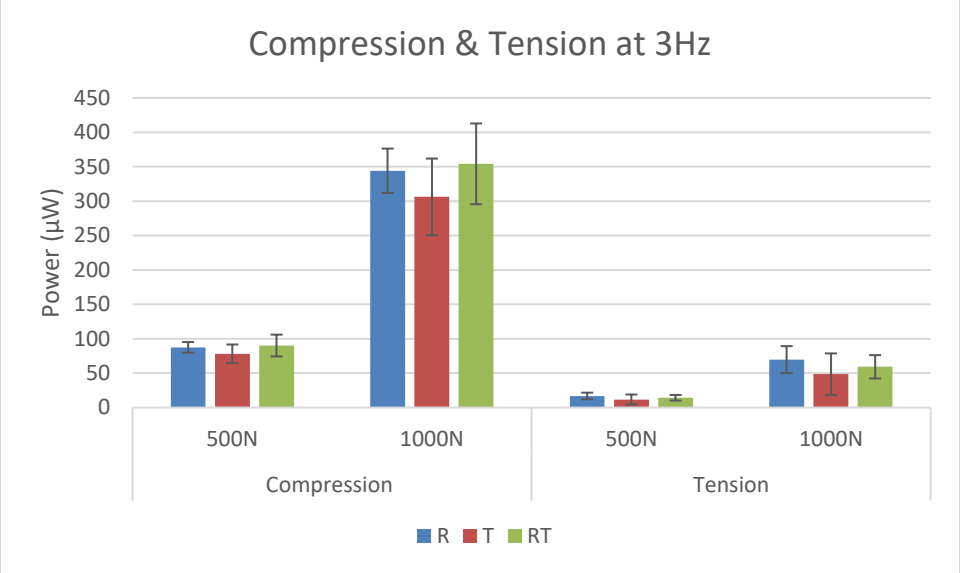

Figure 4: *Effect of compression or tension on power generation of three types of CLACS: radial-poled (R), through-poled (T), and radial-through-poled (RT).*
Power represents the maximum power generated at 3Hz for each specimen. Each bar represents the mean ± SD of 4-5 CLACS.

Table 5: *Effect of compression or tension on power generation.*
Power represents the maximum power generated at 3Hz for each specimen. Each value represents the mean ± SD of 4-5 CLACS.

		R	T	RT
		Power ± SD (µW)	**Power ± SD (µW)**	**Power ± SD (µW)**
Compression	**500N**	87.6 ± 7.75	78.2 ± 13.5	90.1 ± 15.8
	1000N	344 ± 32.3	306 ± 55.7	354 ± 58.7
Tension	**500N**	16.9 ± 4.82	11.7 ± 7.27	14.3 ± 4.03
	1000N	69.7 ± 19.7	48.6 ± 30.1	59.2 ± 17.0

Table 6: *Effect of compression or tension on the coefficient of variation (CV) for the three types of CLACS.*

CV (%)	Load	R	T	RT
Compression	**500N**	8.85	17.2	17.6
	1000N	9.38	18.2	16.6
Tension	**500N**	28.6	61.9	28.2
	1000N	28.2	62.1	28.6

Effect of Ultrasound

The effect of ultrasound on power generation by the three types of CLACS is shown in Figure 5 and Table 7. As ultrasound intensity increases from 0.1 W/cm^2 to 1 W/cm^2 at 0° and 90° orientations, the average maximum power generation increases. Ultrasound intensity of 0.1 W/cm^2 in all CLACS produced between 3μW to 30μW of power. The R-CLACS tended to produce approximately twice the power than the T-CLACS and RT-CLACS produced at the 0° orientation, however, at both the 0° orientation and the 90° orientation, no statistical difference in power generation was observed between the three types of CLACS.

Power generation of the CLACS by ultrasound at the 90° orientation is much less than at the 0° orientation. For example, as shown in Table 7, the power generated by 0.1 W/cm^2, 0.5 W/cm^2, and 1 W/cm^2 by ultrasound loading at the 0° orientation is approximately 4 times, 4 to 7 times, and 3 to 8 times more, respectively, than the power generated at the 90° orientation.

The coefficient of variation (CV) observed after ultrasound loading was large, averaging 66%, and ranging from 26% to 109%. The T-CLACS show a somewhat smaller mean CV of 49% than either the R-CLACS and RT-CLACS, with a mean CV of approximately 75%.

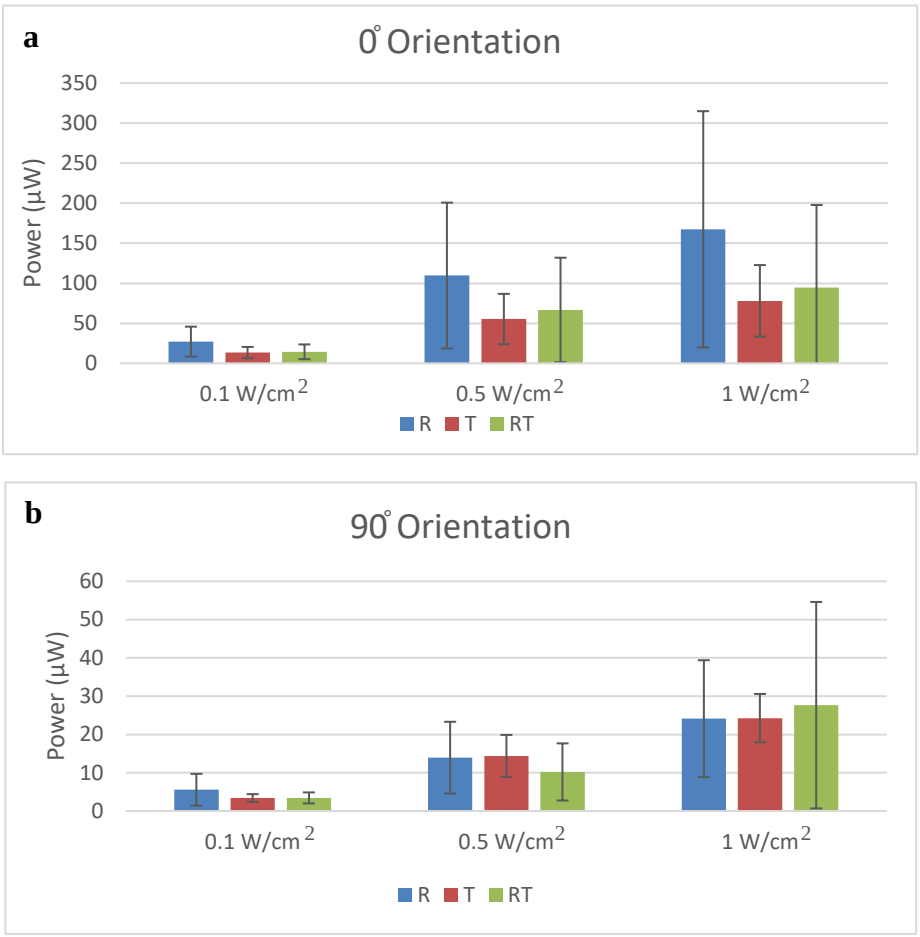

Figure 5: *Effect of ultrasound on power generation of three types of CLACS: radial-poled (R), through-poled (T), and radial-through-poled (RT).*
Figure 5a and 5b illustrates the power generated from the 0° and 90° orientation of the transducer head relative to the medial axis of the CLACS. Data represents mean ± SD of 5 CLACS.

Table 7: *Effect of ultrasound on the power generation of three types of CLACS: radial-poled (R), through-poled (T), and radial-through-poled (RT).*
Data (mean ± SD) is the power generated from the 0° and 90° orientation of the transducer head relative to the medial axis of the CLACS.

Intensity	**CLACS Type**	**0° Orientation**	**90° Orientation**
		Power ± SD (µW)	**Power ± SD (µW)**
0.1 W/cm²	**R**	27.1 ± 18.7	5.6 ± 4.15
	T	13.4 ± 7.08	3.40 ± 1.01
	RT	14.4 ± 9.25	3.43 ± 1.44
0.5 W/cm²	**R**	109 ± 91.1	13.9 ± 9.37
	T	55.3 ± 31.5	14.4 ± 5.49
	RT	66.7 ± 65.2	10.2 ± 7.46
1.0 W/cm²	**R**	167 ± 148	24.1 ± 15.3
	T	78.0 ± 44.7	24.3 ± 6.31
	RT	94.5 ± 103	27.7 ± 27.0

Table 8: *Effect of ultrasound on the coefficient of variation (CV) for the three types of CLACS.*

Intensity	Specimen Type	0° (%)	90° (%)
0.1 W/cm²	**R**	69.2	74.7
	T	52.9	29.6
	RT	64.3	41.9
0.5 W/cm²	**R**	83.1	67.2
	T	56.8	38.2
	RT	97.8	73.1
1.0 W/cm²	**R**	88.2	63.4
	T	57.3	26.0
	RT	109	97.5

Discussion

Regenerative medicine is the application of new drugs, tissues, and other methods to aid in the prevention and recovery from various human diseases and ailments. One major condition associated with aging is the deterioration and breakage of bones. The environment of some fractures is not conducive to healing, especially with those who have comorbidities such as osteoporosis and diabetes. In response to this need, our research is aimed to fill this gap by examining the usefulness of electrical stimulation from piezoelectric materials, not only for the repair of bones, but also for the repair of soft tissues.

The purpose of this study was to examine two unconventional modes of loading on power generation of three types of CLACS, namely R-CLACS, T-CLACS, and RT-CLACS. The most common type of loading is compression, but in these studies, we examined tension and ultrasound as non-traditional modes of loading.

It is known that the CLACS produce power at much lower resistances than monolithic piezoelectric elements (Platt et al., 2005). Therefore, it was of interest to characterize the three

types of CLACS in the present study using a resistance sweep. As shown in Figure 1, all three types of CLACS reach a maximum power generation around 2 MΩ of resistance.

Little is known on the effects of tension on piezoelectric materials. Tension is a mode of loading found within the human body, and it is vital to know how the CLACS respond to tension, as to further understand factors that might affect the functionality of CLACS. Therefore, to determine the effect of tension loading on power generation, three amplitudes with four frequencies of tension loading were used. Figure 2 and Table 1 demonstrate the power generation for each CLACS type under various tension loads. A trend of increasing power generation was noted as the frequency increased from 0.5Hz to 3Hz. This is due to the impedance of piezoelectric materials, which produce more power at higher frequencies (Platt et al., 2005). At the load amplitudes of 100N, 500N, and 1000N, the power produced was less than 17μW for the two lower amplitudes, and up to 70μW for the 1000N amplitude. The power produced by the two lower amplitudes of tension are probably insufficient for stimulating bone growth but may be sufficient for promotion of soft tissue healing. The average human walk produces approximately 2Hz of loading, while the average human run produces approximately 3Hz of loading (Ji & Pachi, 2005). The highest power generation produced by 2Hz and 3Hz at 1000N of tension in the present study was found with the R-CLACS producing 44μW and 70μW, respectively. It is therefore possible to utilize the R-CLACS during 2Hz and 3Hz at 1000N of tension to generate power, but it is unlikely to be used for bone stimulation, due the relatively low power generation and the high CV.

In this study we examined whether the poling direction effected the amount of power generated under the same tension loads. The R-CLACS are radial-poled, the T-CLACS are through-thickness poled, and the RT-CLACS consist of both radial-poled and through-poled

disks. As shown in Table 1, no statistical difference of power generation was found between the R-CLACS, T-CLACS, and RT-CLACS at any of the tension loads. Table 2 shows the CV of the various tension loading conditions, averaging approximately 38%. The highest CV was noted with the T-CLACS, with a mean CV of 62%, compared to the R-CLACS and RT-CLACS that had a mean CV of approximately 26%.

To further investigate the effect of tension on CLACS, each specimen was tested using compression before and after the tension study. When designing piezoelectric structures, the most used mode of loading is compression, for its ability to generate power most efficiently. Figure 3 shows the power generation for all three CLACS under two amplitudes of compression and two frequencies of loading. The compression tests produced 14% less power after tension than before tension. An ANOVA test ($\alpha<0.05$) showed that the only statistically significant difference between the pre- and post-tension compression was found in R-CLACS under loading conditions of 1000N. The trend of lower power generation found in the post-tension test could be due to delamination of the piezoelectric elements from the compliant layers. In compression, the radial strain is increased due to the compliant layers (Cadel et al., 2018). If delamination was occurring during tension loading, the bonding forces between the piezoelectric disks and the compliant layers would be reduced. A significant decrease in power generation from the pre- to post-tension tests were observed for the R-CLACS (Figure 2), where most of the energy being produced is from radial strain due to poling direction.

As noted previously, compression loading is the most common method of producing power from piezoelectric materials. Therefore, it was of interest to compare the ability of tension loading to compression loading of power generation in the three types of CLACS. As shown in Figure 4 and Table 5, tension loading produced only 17% of the power produced by compression

loading, and the CV for the tension loading was much higher (40%) than compression loading (15%).

Ultrasound is another potential unconventional mode of loading piezoelectric materials to generate power. In this study the effect of two transducer orientations of ultrasound wave energy to generate power form the CLACS was examined. Ultrasound machines utilize electricity and piezoelectric crystals to produce ultrasound waves that transport mechanical energy (Tsaklis, 2010). In theory, the mechanical energy of ultrasound waves could be used to generate electricity from PZT disks. If a bedridden patient has received an implant with a CLACS system, the benefit of CLACS would be minimized due to little opportunity for mechanical loading. In contrast, ultrasound loading might be an alternative to mechanical loading, ensuring bedridden patients have the benefit of CLACS.

Overall, the power generation data gathered from the ultrasound testing of the CLACS system is low with high variance. The high variance of ultrasound testing is probably due to a variety of factors, such as the unpredictability of the ultrasound waves being attenuated as they pass through the ultrasound phantom. The ultrasound phantom was made from a highly concentrated edible gelatin mixture that is temperature dependent. When placed under ultrasonic loads, the temperature within the phantom can increase, making the gelatin mixture soften or in extreme cases liquefy, changing the attenuation properties of the material. The ultrasound transducer was fixed in place by observing the sign wave produced by the CLACS element before testing began, which could introduce inconsistency with total power output of the system. The variance is especially high for the RT-CLACS in ultrasound. It is known that most of the energy of ultrasound waves is absorbed by the first couple disks in CLACS (Alters, 2019), and the poling direction of the top disks are different in the RT-CLACS used in this study.

As shown in figure 5 and Table 3, as the intensity of the ultrasound increases, the power generated by the CLACS also tends to increase. For example, at 0° orientation, the average power generated at 0.1 W/cm^2, 0.5 W/cm^2, and 1 W/cm^2 was 18μW, 77μW, and 113μW, respectively. At the 90° orientation, the power generated was much less than at 0°, with 0.1 W/cm^2, 0.5 W/cm^2, and 1 W/cm^2 producing a mean of 4μW, 13μW, and 25μW, respectively. The low power generation produced by ultrasound at the 90° orientation, confirms that shown by Alters (Alters, 2019). The trend of increasing power generation as ultrasound intensity increases is due to the frequency of vibration of the disk growing closer to its resonance frequency, the frequency that a piezoelectric material is vibrating most readily (APC International, 2011). The CV of power generation for ultrasound loading is very high, with a mean of 66%. Ultrasound loading at the 90° orientation throughout all intensities examined produced less than 28μW, suggesting that the power generated would be insufficient to enhance bone repair. However, at the 0° orientation, 0.5 W/cm^2 and 1 W/cm^2 produced a mean power generation of 79μW and 85μW, respectively. Therefore the 0° orientation is more likely to be beneficial for enhancing bone repair than the 90° orientation.

In all the loading studies described above three types of CLACS were employed, namely the R-CLACS, T-CLACS, and RT-CLACS, and it was of interest to determine their relative performance. In the tension loading experiments, the R-CLACS showed a trend of higher power generation than the other CLACS. In the experiments where compression loading was performed before and after tension loading, the R-CLACS produced significantly less power post-tension loading than the other two CLACS, and the CV for the T-CLACS was larger than the other two CLACS. In the ultrasound loading experiments at the 0° orientation, R-CLACS tended to produce approximately twice the power than the other two CLACS. Thus, there are not marked

differences in performances of the three CLACS. However, in the tension loading and ultrasound loading experiments the R-CLACS tended to outperform the other CLACS, but when tension loading was introduced, the power generated by the second compression loading was significantly less in the R-CLACS in comparison to that produced by the other CLACS.

Conclusion

Non-traditional loading by tension and ultrasound on the piezoelectric CLACS system was examined. Tension resulted in low power generation in comparison to that produced by compression. The effect of tension on power generation by compression was only slightly decreased. Ultrasound loading was conducted at 0° and 90° orientations. At the 90° orientation little or no power was generated. However, at the 0° orientation power was generated but was much less than by compression. Because the power generated by both tension and ultrasound are much less than by compression, these two non-traditional loads are more likely to be usable for soft tissue than bone healing.

References

Alters, M. (2019). *Determination of clinical efficacy of ultrasound stimulation on piezoelectric composites for power generation applications* University of Kansas]. ProQuest Dissertations Publishing.

APC International, L. (2011). *Piezoelectric Ceramics: Principles and Applications*. APC International. https://books.google.com/books?id=nUafpwAACAAJ

Baranowski, J. T. J., Black, J., Brighton, C. T., & Friedenberg, Z. B. (1983). Electrical osteogenesis by low direct current. *Journal of Orthopaedic research*, *1*(2), 120-128.

Brighton, C. T., Black, J., Friedenberg, Z., Esterhai, J., Day, L., & Connolly, J. (1981). A multicenter study of the treatment of non-union with constant direct current. *JBJS*, *63*(1), 2-13.

Cadel, E. S., Krech, E. D., Arnold, P. M., & Friis, E. A. (2018). Stacked PZT discs generate necessary power for bone healing through electrical stimulation in a composite spinal fusion implant. *Bioengineering*, *5*(4), 90.

Cain, M., Stewart, M., & Gee, M. (1999). Degradation of Piezoelectric Materials. *NPL Report CMMT(A) 148*, 1-42.

Calori, G. M., Mazza, E. L., Mazzola, S., Colombo, A., Giardina, F., Romanò, F., & Colombo, M. (2017). Non-unions. *Clinical Cases in Mineral and Bone Metabolism*, *14*(2), 186.

Carter, R., & Kensley, R. Introduction to Piezoelectric Transducers. *Midé Technology Corp., Woburn, MA. Google Scholar*.

Cochran, G., Johnson, M., Kadaba, M., Vosburgh, F., Ferguson-Pell, M., & Palmeiri, V. (1985). Piezoelectric internal fixation devices: A new approach to electrical augmentation of osteogenesis. *Journal of Orthopaedic research*, *3*(4), 508-513.

Cottrill, E., Pennington, Z., Ahmed, A. K., Lubelski, D., Goodwin, M. L., Perdomo-Pantoja, A., Westbroek, E. M., Theodore, N., Witham, T., & Sciubba, D. (2019). The effect of electrical stimulation therapies on spinal fusion: a cross-disciplinary systematic review and meta-analysis of the preclinical and clinical data. *Journal of Neurosurgery: Spine*, *32*(1), 106-126.

Duda, G. N., Schneider, E., & Chao, E. Y. (1997). Internal forces and moments in the femur during walking. *J Biomech*, *30*(9), 933-941. https://doi.org/10.1016/s0021-9290(97)00057-2

Falyar, C. R. (2017). *Reflection, Refraction, Scattering, and Attenuation*. https://www.vaultrasound.com/educational-resources/ultrasound-physics/reflection-refraction/

Franklin, B. M., Maroudas, E., & Osborn, J. L. (2016). Sine-wave electrical stimulation initiates a voltage-gated potassium channel-dependent soft tissue response characterized by induction of hemocyte recruitment and collagen deposition. *Physiol Rep*, *4*(12), e12832-n/a. https://doi.org/10.14814/phy2.12832

Friis, E. A., Galvis SN, & PM, A. (2015). DC stimulation for spinal fusion with a piezoelectric composite material interbody implant: An ovine pilot study. *Society For Biomaterials*.

Fukada, E., & Yasuda, I. (1957). On the Piezoelectric Effect of Bone. *Journal of the Physical Society of Japan*, *12*(10), 1158-1162. https://doi.org/10.1143/JPSJ.12.1158

Goetzinger, N. C., Tobaben, E. J., Domann, J. P., Arnold, P. M., & Friis, E. A. (2016). Composite piezoelectric spinal fusion implant: Effects of stacked generators. *J Biomed Mater Res B Appl Biomater*, *104*(1), 158-164. https://doi.org/10.1002/jbm.b.33365

Griffin, M., & Bayat, A. (2011). Electrical stimulation in bone healing: critical analysis by evaluating levels of evidence. *Eplasty*, *11*.

Guerin, S., Tofail, S. A., & Thompson, D. (2019). Organic piezoelectric materials: milestones and potential. *NPG Asia Materials*, *11*(1), 1-5.

Holmes, D. (2017). Non-union bone fracture: a quicker fix. *Nature*, *550*(7677), S193-S193.

Huang, C., & Ogawa, R. (2010). Mechanotransduction in bone repair and regeneration. *The FASEB Journal*, *24*(10), 3625-3632.

Ji, T., & Pachi, A. (2005). Frequency and velocity of people walking. *Structural Engineer*, *84*(3), 36-40.

Kooiman, K., Roovers, S., Langeveld, S. A. G., Kleven, R. T., Dewitte, H., O'Reilly, M. A., Escoffre, J. M., Bouakaz, A., Verweij, M. D., Hynynen, K., Lentacker, I., Stride, E., & Holland, C. K. (2020). Ultrasound-responsive cavitation nuclei for therapy and drug delivery. *Ultrasound Med Biol*, *46*(6), 1296-1325. https://doi.org/10.1016/j.ultrasmedbio.2020.01.002

Krech, E. D., Cadel, E. S., Barrett, R. M., & Friis, E. A. (2018). Effect of compliant layers within piezoelectric composites on power generation providing electrical stimulation in low frequency applications. *J Mech Behav Biomed Mater*, *88*, 340-345. https://doi.org/10.1016/j.jmbbm.2018.08.027

Leighton, T. G. (2007). What is ultrasound? *Progress in Biophysics and Molecular Biology*, *93*(1), 3-83. https://doi.org/https://doi.org/10.1016/j.pbiomolbio.2006.07.026

Loi, F., Córdova, L. A., Pajarinen, J., Lin, T.-h., Yao, Z., & Goodman, S. B. (2016). Inflammation, fracture and bone repair. *Bone*, *86*, 119-130.

Lowrie, F. C., MG; Stewart, M; Gee MG. (1999). *Time dependent behaviour of piezo-electric materials* [NPL Report]. http://eprintspublications.npl.co.uk/1059/

Marin, C., Luyten, F. P., Van der Schueren, B., Kerckhofs, G., & Vandamme, K. (2018). The impact of type 2 diabetes on bone fracture healing. *Frontiers in Endocrinology*, *9*, 6.

Ogden, J. A., Tóth-Kischkat, A., & Schultheiss, R. (2001). Principles of shock wave therapy. *Clin Orthop Relat Res*(387), 8-17. https://doi.org/10.1097/00003086-200106000-00003

Platt, S. R., Farritor, S., & Haider, H. (2005). On low-frequency electric power generation with PZT ceramics. *IEEE/ASME Transactions on Mechatronics*, *10*(2), 240-252. https://doi.org/10.1109/TMECH.2005.844704

Ruff, C., Holt, B., & Trinkaus, E. (2006). Who's afraid of the big bad Wolff?:"Wolff's law" and bone functional adaptation. *American Journal of Physical Anthropology*, *129*(4), 484-498.

Salter, D., Robb, J., & Wright, M. (1997). Electrophysiological responses of human bone cells to mechanical stimulation: evidence for specific integrin function in mechanotransduction. *Journal of Bone and Mineral Research*, *12*(7), 1133-1141.

Schumacher, D., Strunz, V., & Gross, U. (1983). Does piezoceramic influence avian bone formation in the early postoperative phase? *Biomaterials*, *4*(3), 215-217.

Sheung-tung, H. (2017). Quit Smoking before Orthopaedic Surgery. *Journal of Orthopaedics, Trauma and Rehabilitation*, *23*(1), A1-A3. https://doi.org/10.1016/j.jotr.2017.10.001

Shriki, J. (2014). Ultrasound physics. *Crit Care Clin*, *30*(1), 1-24, v. https://doi.org/10.1016/j.ccc.2013.08.004

Tsaklis, P. (2010). Presentation of acoustic waves propagation and their effects through human body tissues. *Human Movement*, *11*. https://doi.org/10.2478/v10038-009-0025-z

van den Ende, D., Bos, B., Groen, P., & Dortmans, L. M. J. G. (2009). Lifetime of piezoceramic multilayer actuators: Interplay of material properties and actuator design. *Journal of Electroceramics*, *22*, 163-170. https://doi.org/10.1007/s10832-007-9411-0

Xin, Z., Lin, G., Lei, H., Lue, T. F., & Guo, Y. (2016). Clinical applications of low-intensity pulsed ultrasound and its potential role in urology. *Transl Androl Urol*, *5*(2), 255-266. https://doi.org/10.21037/tau.2016.02.04

Zhang, S., Xia, R., & Shrout, T. R. (2007). Lead-free piezoelectric ceramics vs. PZT? *Journal of Electroceramics*, *19*(4), 251-257.

Zura, R., Xiong, Z., Einhorn, T., Watson, J. T., Ostrum, R. F., Prayson, M. J., Della Rocca, G. J., Mehta, S., McKinley, T., & Wang, Z. (2016). Epidemiology of fracture nonunion in 18 human bones. *JAMA surgery*, *151*(11), e162775-e162775.

Chapter 4: Conclusions and Future Work

Characterization of the piezoelectric CLACS system under non-traditional loading was examined to better understand their power generation in comparison to compression loading. Tension loading resulted in low power generation, indicating the effect of CLACS is not utilized under tension loading. Tension loading tended to lower power generation by compression loading. Although not statistically significant, the trend suggest that slight delamination might occur when CLACS are introduced to tension loads. Ultrasound loading was examined at the 0° and 90° orientations. Ultrasound loading at the 90° orientation produced little or no power. Whereas ultrasound loading in the 0° orientation theoretically produced power with intensities for some therapeutic applications. In comparing the three CLACS used in this study, the R-CLACS tended to generate more power than the two other CLACS, although not statistically significant. Overall, this study shows the usability for the CLACS system for nontraditional loading conditions.

When designing an implant utilizing the CLACS system, one must consider all loading conditions within the human body. This research shows natural loading in tension is probably not a viable way to generate power for aiding in bone growth. It is also shown that CLACS tend to produce less power during compression post-tension loading. Compression should be isolated when designing the CLACS system into an implant, or the CLACS system needs to be redesigned to account for tension. One possible way to design the CLACS system for tension loading is to increase the adhesive forces between the compliant layers and PZT disks. This increase in adhesive force could be found by testing different types of adhesives or changing the surface characteristics of the disks. Increasing the adhesive forces between the PZT disks and compliant layers will decrease the likelihood of delamination.

Overall, the study is limited by the variance seen throughout tension and ultrasound loading. The variance could be caused by a variety of factors such as specimen age, angle of CLACS, ultrasound phantom properties, and ultrasound beam uniformity. The CLACS were made approximately two years prior to this study by Dr. Ember Krech (Krech, 2020). Over time, the CLACS poling direction could have been affected due to storing environment. When the CLACS were made, the angle of the stack inside the epoxy shell varied in relation to the medial axis. Potential for power generation is highest when poling direction is parallel to strain in piezoelectric materials (APC International, 2011). If the CLACS is not fully aligned to the direction of load, this could introduce variance within power generation. The ultrasound phantoms material properties were temperature dependent. As ultrasound waves travel to the CLACS system, some of the mechanical energy is absorbed as heat energy. The gelatin's attenuation properties could be affected by an increase of temperature, likely introducing variance. The therapeutic ultrasound machine generated a non-uniform ultrasound beam, with a beam non-uniformity ratio (BNR) of 5:1. The BNR represents the peak intensity verses the average intensity of the ultrasound beam. This beam non-uniformity could have introduced variance while aligning the ultrasound transducer with the orientation of the CLACS.

The increase of ultrasound variance could be due to the material properties of the ultrasound phantom. The gelatin mixture was water-based, making its material properties temperature dependent. During ultrasound loading the gelatin absorbs some of the mechanical energy of the ultrasound waves creating heat within the phantom, changing the attenuation of the ultrasound wave. Other gelatins were researched to avoid this problem. An oil-based gelatin called Gelatin #0 (Humimic Medical, Greenville, SC), could withstand the heat produced from the ultrasound waves without changing attenuation properties. The properties of Gelatin #0

closely match those of soft tissue. When testing Gelatin #0, air bubbles formed around the CLACS while imbedding the specimen inside the gelatin. Air bubbles absorb energy from the ultrasound waves, lowering the amount of energy transferred to the CLACS. Gelatin #0 is a viable option to replace the current water-based ultrasound phantom and should be further tested to reduce variance in ultrasound loading of CLACS.

In the future, more testing must be done to fully understand the source of variance for all studies. Making updated CLACS, ensuring the inner stack is aligned with the medial line of the specimen and using a larger sample size, the variance of tension could be further understood. Tension loading CLACS at higher frequency and loading amplitudes could further expand the use of tension for new applications outside the human body. By developing an ultrasound phantom to be more consistent than the present study, the variance could be reduced.

Appendix A: Detailed Methods

Tension Loading

1. Once finished with first round of compression, continue with tension loading took place.
2. Test impedance and capacitance using a Hioki 3522-50 LCR HiTester (Hioki, Plano, TX) at 3Hz and 5Hz to later compare values after tension and ultrasound to help clarify the validity of the specimens.
3. Calibrate and warm-up the biaxial MTS machine.
4. Place one specimen into the jaws of the MTS, clamping the bottom.
5. Attach resistance sweep alligator clips to the specimen.

a. The resistance sweep set up consists of a resistance box, where the negative lead is attached directly to the specimen. The positive of the resistance box is attached to the positive of the MTS AUX channel. The negative of the AUX channel is attached directly to the specimen. Bridging the gap between the negative and positive channels of the MTS AUX, there is a 26 K Ohm resistor. Its purpose is to help clean noise from the cable.

6. Move the top jaw down and grip the top of the specimen.
7. Name the specimen uniquely with date, type of loading, and specimen name (ie. 2020_06_11_tension_R5)
8. Start collection, changing the resistance value as the resistance sweep progresses.
9. Save the data on an external flash drive to use for MATLAB code.
10. Analyze raw data through MATLAB code and save data in excel files.
11. Use Excel files to graph Force Range(N), Resistance (Ohms), Voltage (V), Power average (W), and Power Max (W).
12. Once finished, repeat steps 2-11 of tension loading for every specimen type.
13. Utilizing an ANOVA test ($\alpha<0.05$) or one-sided Wilcoxon Rank Sum test ($\alpha>0.05$), determine if data is statically significantly different between poling directions.

Compression Loading

All compression loading procedure was modified from Dr. Ember Krech(Krech 2020).

1. Obtain compliant layer adaptive composite stacks (CLACS) from Ember Krech, consisting of 5 through poled disks, 5 mix-mode CLACS (MMCLACS) with radial and through poled disks, and 5 radially poled disks. All disks are 0.8 mm thick with the same thickness of compliant layer between them.
2. Test impedance and capacitance using a Hioki 3522-50 LCR HiTester (Hioki, Plano, TX) at 3Hz and 5Hz to later compare values after tension and ultrasound to help clarify the validity of the specimens.
3. Calibrate and warm-up the biaxial MTS machine.
4. Place one specimen into the jaws of the MTS, clamping the bottom.
5. Attach resistance sweep alligator clips to the specimen.

a. The resistance sweep set up consists of a resistance box, where the negative lead is attached directly to the specimen. The positive of the resistance box is attached to the

positive of the MTS AUX channel. The negative of the AUX channel is attached directly to the specimen. Bridging the gap between the negative and positive channels of the MTS AUX, there is a 26 K Ohm resistor. Its purpose is to help clean noise from the cable.

6. Move the top jaw down and grip the top of the specimen.
7. Name the specimen uniquely with date, type of loading, and specimen name (ie. 2020_06_11_comp1_R5)
8. Start collection, changing the resistance value as the resistance sweep progresses.
9. Save the data on an external flash drive to use for MATLAB code.
10. Repeat steps 2-9 for every specimen type.
11. Analyze through MATLAB code and save data in excel files.
12. Use Excel files to graph Force Range(N), Resistance (Ohms), Voltage (V), Power average (W), and Power Max (W).
13. Repeat 2-13 post-tension loading.
14. Use an ANOVA test ($\alpha<0.05$) to understand statistical differences of pre- and post-tension loading.

Ultrasound Loading

All ultrasound loading procedure was modified from Morghan Alters (Alters 2019).

1. Cut specimens down, so approximately 5 mm of epoxy is between the outside face and the end of the Piezoelectric stack.
2. Two containers are made to hold the specimen at 90 degrees and 0 degrees are used to suspend a specimen, using a think plastic sheet for the side where the transducer will be placed.
3. Fill the containers with gelatin and leave in refrigerator for 1 to 2 hours to solidify.
4. Before starting testing turn on both the ultrasound machine and the oscilloscope for 5 minutes to warm.
5. Plug a flash drive into the oscilloscope to save files.
6. Then set the oscilloscope to record 2000 data points with a scale of 2 microseconds
7. Set the file to record in .CSV, then set the name of the file to read the specimen type, angle, intensity, resistance (ie. R4_0d_01_01)
8. Remove specimen from refrigerator and attach alligator clips to positive and negative lead of the specimen.
9. Connect Coaxial Cable BNC connector to channel 1 of the oscilloscope. Connect the positive lead of the Coaxial cable to the output of the RC Box, and the negative lead to the specimen. Then connect the input of the RC Box to the other lead of the specimen.
10. Clamp the ultrasound transducer in place at either the 0° or 90° orientations.
11. Apply a thin uniform layer of ultrasound coupling gel on the head of the transducer and the thin plastic film of the testing container.
12. Set the ultrasound machine to a continuous loading frequency of 1 MHz.
13. Depending on loading condition trial, set the ultrasound intensity to $0.1\ \mathrm{W/cm^2}$, $0.5\ \mathrm{W/cm^2}$, or $1\ \mathrm{W/cm^2}$.
14. Press the start on the ultrasound machine to start testing.

15. Leave ultrasound machine running for approximately 15 seconds, then save the waveform on the oscilloscope.
16. Stop the ultrasound machine for 15 seconds and change resistance on RC box.
17. Repeat steps 14-16 until resistance sweep is completed for the chosen loading condition.
18. Repeat steps 14-17 until all intensity loading conditions are completed for one orientation of the ultrasound transducer.
19. Make new gelatin mixture and repeat steps 3-18 for second ultrasound transducer orientation.
20. Analyze through MATLAB code and save data in excel files.
21. Use Excel files to graph Resistance (Ohms), Voltage (V), Power average (W), and Power Max (W).
22. Use an ANOVA test ($\alpha<0.05$) to understand statistical differences between poling direction of disks, and orientation angle.

Gelatin Mixture

1. Fill beaker with 237mL (~1 Cup) of deionized water and place on hotplate set to 180℃ for 3-5 minutes to warm water.
2. Mix in three 0.25oz packets of gelatin power to warm water. Using a stir bar, mix gelatin for 10 minutes.
3. Remove beaker from the hotplate, inspect the mixture to ensure the gelatin powder is fully mixed, and let sit for 30 minutes.
4. Suspend the specimen ensuring it is 20mm away from the thin plastic sheet side of the testing container.
5. Pour the gelatin mixture into the container and place into the refrigerator for 1-2 hours to set gelatin.
6. Remove testing container and specimen from the refrigerator and ensure the conductive leads of the specimen are not touching the gelatin.
8. The specimen is now ready for ultrasound testing.

Resistance Sweep Values

Tension	Compression	Ultrasound
0 Ω	0.05 MΩ	1 Ω
0.025 MΩ	0.35 MΩ	2 Ω
0.05 MΩ	0.55 MΩ	2.7 Ω
0.1 MΩ	0.75 MΩ	4.7 Ω
0.2 MΩ	0.95 MΩ	10 Ω
0.35 MΩ	1 MΩ	13 Ω
0.45 MΩ	1.5 MΩ	15 Ω
0.55 MΩ	2 MΩ	20 Ω
0.65 MΩ	3 MΩ	25 Ω
0.75 MΩ	5 MΩ	35 Ω
0.85 MΩ	6.5 MΩ	45 Ω
0.95 MΩ	7.5 MΩ	60 Ω
1 MΩ	9 MΩ	75 Ω
1.5 MΩ		100 Ω
2 MΩ		125 Ω
2.5 MΩ		150 Ω
3 MΩ		200 Ω
3.5 MΩ		250 Ω
4 MΩ		300 Ω
4.5 MΩ		350 Ω
5 MΩ		
5.5 MΩ		
6 MΩ		
6.5 MΩ		
7 MΩ		
7.5 MΩ		
8 MΩ		
8.5 MΩ		
9 MΩ		
9.5 MΩ		
10 MΩ		
12 MΩ		
14 MΩ		
16 MΩ		
18 MΩ		
20 MΩ		

Appendix B: MATLAB Code

Tension Loading MATLAB Code

```
%Data Analysis for Testing Piezoelectric Composites in
Tension
%Originally written by John Doman in 2013 (For compression
loading)
%Updated by Ember Krech in September 2018 (For compression
loading)
%Edited by Luke Lindemann in 2020 (For tension loading)


%*****TENSION LOADING ON BIAXIAL MACHINE******
%Clear data
clear
close all
clc

%***Be sure to change specimen_name and file_location and
Rmts if necessary
%***FOR MIXED SPECIMEN


%% Input Parameters

%**This should be updated if you add resistors when voltage
signal saturates

%Rmts = 2E6; %ohms %fixed MTS electrical resistance
Rmts = 79e3; %ohms %there is one resistor (1 kohm) in
parallel with the 2E6 resistance

%MAKE SURE TO DOUBLE CHECK THE RESISTANCE SWEEP VALUES!

numCatch = 0;
%% Load Desired Data
count = 1;
specimen_name = ['Tension_Example']; %desired filename for
the excel file with analyzed data
file_location = ['F:\Tension_Example\']; %raw MTS data file
location
output_file = ['Data ' specimen_name];
```

```
%This is the complete resistance sweep (37 resistances from
.025Mohm to 20Mohm) - modify line 35 as necessary
Resistance_Sweep = [0  0.025e6 0.05e6 0.1e6 0.2e6 0.35e6
0.45e6 0.55e6 0.65e6 0.75e6 0.85e6 0.95e6 1e6 1.5e6 2e6
2.5e6 3e6 3.5e6 4e6 4.5e6 5e6 5.5e6 6e6 6.5e6 7e6 7.5e6 8e6
8.5e6 9e6 10e6 12e6 14e6 16e6 18e6 20e6];
load = [1 2 3];%number of loads used (100N, 500N, 1000N)
frequency = [1 2 3 5]; %number of frequencies used for each
loading cycle (1Hz, 2Hz, 3Hz, 0.5Hz)


freqCount = 0;
for iFreq = 1:length(frequency)

    freqCount = freqCount +1;

    for iLoad = 1:length(load)

        for iResistor = 1:length(Resistance_Sweep)

%             iFreq = 3;   %You can change these to look at
specific data
%             iLoad = 1;
%             iResistor = 31;

            name=[file_location 'specimenXX_load_'
num2str(load(iLoad),'%.1d') '_'
num2str(frequency(iFreq),'%.2d') 'Hz_Rl_'
num2str(iResistor,'%.2d.dat')];
            Reference_column(iLoad,iFreq,iResistor) =
{['specimenXX_load_' num2str(iLoad,'%.1d') '_'
num2str(iFreq,'%.2d') 'Hz_Rl_' num2str(iResistor,'%.2d')]};

            dat = dlmread(name,'\t',5,0); %read in MTS data
files

            Rvar = Resistance_Sweep(iResistor);


            %Store the data values into individual
variables
            time = dat(:,1);
            axial_count = dat(:,2);
```

```
            axial_count = axial_count - min(axial_count)
+1;
            x = -dat(:,3)*10^-3;   %m
            F = -dat(:,4);     %N
            voltage = dat(:,6);   %Volt
%
%             Plot raw voltage data
%             figure(1)
%             plot(x)
%             plot(F)

            %% Filter the data to eliminate excess noise

            %Calculate the sample frequency
            deltaT = diff(time);
            DeltaT = mean(deltaT);
            fs = 1 / DeltaT;

            %initial variables to use a low pass
butterworth filter
            %fc = 8; %Hz - cuttoff frequency
            fc=12;
%
%             if iFreq == 1
%                 fc = 4;       %Hz - cuttoff frequency
%             elseif iFreq == 2
%                 fc = 6;
%             elseif iFreq == 3
%                 fc = 8;
%             else
%                 fc = 10;
%             end
%
            %filter the data to eliminate the excess noise.
filter all data so
            %that they are subject to the same phase delay
                [b,a] = butter(5,2*fc/fs);
                x  = filtfilt(b,a,x);
                F = filtfilt(b,a,F);
                Vmts = filtfilt (b,a,voltage);

                %Plot filtered voltage data

%                 figure(2)
```

```
%                 subplot(2,1,1), plot(voltage)
%                 subplot(2,1,2), plot(Vmts)

            %Eliminate the initial and final portions of
the data
            %The MTS collects 15 cycles of each force, at
each frequency,
            %we only want to analyze the middle section
(steady-state)

            time = time(axial_count > 5 & axial_count <
27);
            x = x(axial_count > 5 & axial_count < 27);
            F = F(axial_count > 5 & axial_count < 27);
            Vmts = Vmts(axial_count > 5 & axial_count <
27);
            axial_count = axial_count(axial_count > 5 &
axial_count < 27);

%             figure(3)
%             plot(Vmts)

            %% Segment the data into 5 loading and
unloading cycles
            %This can be used to calcualte specimen
stiffness, and d33/g33
            %loading cycles
            cycle1 = [10:2:18];

            time = time(axial_count >= min(cycle1) &
axial_count <= max(cycle1));
            x = x(axial_count >= min(cycle1) & axial_count
<= max(cycle1));
            F = F(axial_count >= min(cycle1) & axial_count
<= max(cycle1));
            Vmts = Vmts(axial_count >= min(cycle1) &
axial_count <= max(cycle1));
            axial_count = axial_count(axial_count >=
min(cycle1) & axial_count <= max(cycle1));

            timeL=time(find(ismember(axial_count,cycle1)));
            xL=x(find(ismember(axial_count,cycle1)));
            FL=F(find(ismember(axial_count,cycle1)));
            VL=Vmts(find(ismember(axial_count,cycle1)));
```

```
timeU=time(find(ismember(axial_count,cycle1+1)));
            xU=x(find(ismember(axial_count,cycle1+1)));
            FU=F(find(ismember(axial_count,cycle1+1)));
            VU=Vmts(find(ismember(axial_count,cycle1+1)));

%                       figure(4)
%                       plot(timeL, VL,'.')
%                       hold on
%                       plot(timeU, VU,'.r')
%                       plot(time, Vmts,'g-')


            %% Analyze Data

            %Now we have 5 middle cycles of filtered and
phase corrected data for
            %each variable. This test was run in g33 setup,
with a variable
            %load resistance. The output voltage and power
for each each
            %resistance can now be analyzed


                        Vmts = Vmts*(1/sqrt(2)); %convert
to RMS voltage
                        Vout = Vmts.*(1+Rvar/Rmts);
%scale voltage by the applied resistance to find voltage
produced by the implant
                        Vamp = (max(Vout) - (min(Vout)))/2;
%calculate voltage amplitude peak-to-peak
                        P = Vout.^2./(Rvar+Rmts);
%instantaneous power
                        Pavg = trapz(time,P) * 1/(max(time)
- min(time));   %average power for all 5 cycles
                        Pmax = Vamp.^2./(Rvar+Rmts);
%peak power per cycle



            %% Store data to output
            output(count,:) = {load(iLoad), [max(F)-
min(F)], frequency(iFreq),...
```

```
                Rvar+Rmts, Vamp, Pavg, Pmax};

            count = count + 1;

           clear Vmts Vmts_shifted Rvar Vamp Pavg Pmax Vout
        end

    end

end


%% Output to an excel sheet for later analysis
output_header = {'Load' 'F-Range (N)' 'Frequency (Hz)'
'Resistance (ohm)' ...
    'Voltage (V)' 'Pavg (W)' 'Pmax (W)'};

output = [output_header; output];

    xlswrite([output_file '.xlsx'], output_header,1, 'A1')
    xlswrite([output_file '.xlsx'],
output(2:length(Resistance_Sweep)+1,:),'Sheet1','A2')

for ii = 2:12
    xlswrite([output_file '.xlsx'], output_header,ii, 'A1')
    xlswrite([output_file '.xlsx'], output((ii-
1)*length(Resistance_Sweep)+2:length(Resistance_Sweep)*ii+1
,:),ii,'A2')
end


xlswrite([output_file '.xlsx'],output,13,'A1')

disp('Done')
```

Compression Loading MATLAB Code

```
%Data Analysis for Testing Piezoelectric Composites in
Compression
%Originally written by John Doman in 2013
%Updated by Ember Krech in September 2018
%Edited by Luke Lindemann in late 2019
```

```
%*****AIM 2 COMPRESSION TESTING ON BIAXIAL MACHINE******
%Clear data
clear
close all
clc

%***Be sure to change specimen_name and file_location and Rmts
if necessary
%***FOR MIXED SPECIMEN


%% Input Parameters
%**This should be updated if you add resistors when voltage
signal saturates


%Rmts = 2E6; %ohms %fixed MTS electrical resistance
Rmts = 82.4e3; %ohms %in parallel with the 2E6 resistance

%MAKE SURE TO DOUBLE CHECK THE RESISTANCE SWEEP VALUES!

numCatch = 0;
%% Load Desired Data
count = 1;
specimen_name = ['Example']; %desired filename for the excel
file with analyzed data
file_location = ['D:\Example\']; %raw MTS data file location
output_file = ['Example_Test'];


%This is the complete resistance sweep (13 resistances from
.05Mohm to 9Mohm) - modify line 35 as necessary
Resistance_Sweep = [0.05e6 0.35e6 0.55e6 0.75e6 0.95e6 1e6 1.5e6
2e6 3e6 5e6 6.5e6 7.5e6 9e6];
load = [2 3];%number of loads used (500N, 1000N)
frequency = [3 5]; %number of frequencies used for each loading
cycle (3Hz, 5Hz)


freqCount = 0;
for iFreq = 1:length(frequency)

    freqCount = freqCount +1;

    for iLoad = 1:length(load)

        for iResistor = 1:length(Resistance_Sweep)
```

```
            name=[file_location 'specimenXX_load_'
            num2str(load(iLoad),'%.1d') '_'
            num2str(frequency(iFreq),'%.2d') 'Hz_Rl_'
            num2str(iResistor,'%.2d.dat')];
           Reference_column(iLoad,iFreq,iResistor) =
{['specimenXX_load_' num2str(iLoad,'%.1d') '_'
num2str(iFreq,'%.2d') 'Hz_Rl_' num2str(iResistor,'%.2d')]};

           dat = dlmread(name,'\t',5,0); %read in MTS data files

           Rvar = Resistance_Sweep(iResistor);


           %Store the data values into individual variables
           time = dat(:,1);
           axial_count = dat(:,2);
           axial_count = axial_count - min(axial_count) +1;
           x = -dat(:,3)*10^-3;   %m
           F = -dat(:,4);     %N
           voltage = dat(:,6);   %Volt
%
%              Plot raw voltage data
%              figure(1)
%              plot(x)
%              plot(F)

              %% Filter the data to eliminate excess noise

              %Calculate the sample frequency
              deltaT = diff(time);
              DeltaT = mode(deltaT);
              fs = 1 / DeltaT;

              %initial variables to use a low pass butterworth
filter
              fc=12;%Hz - cuttoff frequency

              %filter the data to eliminate the excess noise.
filter all data so
              %that they are subject to the same phase delay
                  [b,a] = butter(5,2*fc/fs);
                  x  = filtfilt(b,a,x);
                  F = filtfilt(b,a,F);
                  Vmts = filtfilt (b,a,voltage);
```

```
                %Plot filtered voltage data

%                 figure(2)
%                 subplot(2,1,1), plot(voltage)
%                 subplot(2,1,2), plot(Vmts)

            %Eliminate the initial and final portions of the
data
            %The MTS collects 15 cycles of each force, at each
frequency,
            %we only want to analyze the middle section (steady-
state)

            time = time(axial_count > 5 & axial_count < 27);
            x = x(axial_count > 5 & axial_count < 27);
            F = F(axial_count > 5 & axial_count < 27);
            Vmts = Vmts(axial_count > 5 & axial_count < 27);
            axial_count = axial_count(axial_count > 5 &
axial_count < 27);

%             figure(3)
%             plot(Vmts)

            %% Segment the data into 5 loading and unloading
cycles
            %This can be used to calcualte specimen stiffness,
and d33/g33
            %loading cycles
            cycle1 = [10:2:18];

            time = time(axial_count >= min(cycle1) & axial_count
<= max(cycle1));
            x = x(axial_count >= min(cycle1) & axial_count <=
max(cycle1));
            F = F(axial_count >= min(cycle1) & axial_count <=
max(cycle1));
            Vmts = Vmts(axial_count >= min(cycle1) & axial_count
<= max(cycle1));
            axial_count = axial_count(axial_count >= min(cycle1)
& axial_count <= max(cycle1));

            timeL=time(find(ismember(axial_count,cycle1)));
            xL=x(find(ismember(axial_count,cycle1)));
            FL=F(find(ismember(axial_count,cycle1)));
            VL=Vmts(find(ismember(axial_count,cycle1)));

            timeU=time(find(ismember(axial_count,cycle1+1)));
```

```
            xU=x(find(ismember(axial_count,cycle1+1)));
            FU=F(find(ismember(axial_count,cycle1+1)));
            VU=Vmts(find(ismember(axial_count,cycle1+1)));

%                   figure(4)

%                   plot(timeL, VL,'.')
%                   hold on
%                   plot(timeU, VU,'.r')
%                   plot(time, Vmts,'g-')


            %% Analyze Data

            %Now we have 5 middle cycles of filtered and phase
corrected data for
            %each variable. This test was run in g33 setup, with
a variable
            %load resistance. The output voltage and power for
each each
            %resistance can now be analyzed


              Vmts = Vmts*(1/sqrt(2)); %convert to RMS voltage
              Vout = Vmts.*(1+Rvar/Rmts);     %scale voltage by
the applied resistance to find voltage produced by the implant
              Vamp = (max(Vout) - (min(Vout)))/2;     %calculate
voltage amplitude peak-to-peak
              P = Vout.^2./(Rvar+Rmts);
%instantaneous power
              Pavg = trapz(time,P) * 1/(max(time) - min(time));
%average power for all 5 cycles
                        Pmax = Vamp.^2./(Rvar+Rmts);
%peak power per cycle



            %% Store data to output
            output(count,:) = {load(iLoad), [max(F)-min(F)],
frequency(iFreq),...
                Rvar+Rmts, Vamp, Pavg, Pmax};

            count = count + 1;

           clear Vmts Vmts_shifted Rvar Vamp Pavg Pmax Vout
        end
```

```
    end

end


%% Output to an excel sheet for later analysis
output_header = {'Load' 'F-Range (N)' 'Frequency (Hz)'
'Resistance (ohm)' ...
    'Voltage (V)' 'Pavg (W)' 'Pmax (W)'};

output = [output_header; output];

    xlswrite([output_file '.xlsx'], output_header,1, 'A1')
    xlswrite([output_file '.xlsx'],
output(2:length(Resistance_Sweep)+1,:),'Sheet1','A2')

for ii = 2:4
    xlswrite([output_file '.xlsx'], output_header,ii, 'A1')
    xlswrite([output_file '.xlsx'], output((ii-
1)*length(Resistance_Sweep)+2:length(Resistance_Sweep)*ii+1,:),i
i,'A2')
end

xlswrite([output_file '.xlsx'],output,5,'A1')

disp('Done')
```

Ultrasound Loading MATLAB Code

```
%% Main Analysis code for analyzation of ultrasound of
MMCLACS
% Written by Luke Lindemann
% Based on Morghan Alters code that was modified by Ember
Krech.
% Last updated: 02/23/2021

clear;close all; clc;

%% Input Parameters
frequency = 1e6;
resistance_sweep=[0 1 0 2 0 3 5 10 15 25 35 50 65 90 115
140 190 240 290 340];

fc= 1.2e6; % cutoff frequency
```

```
%% File Reading

file_path = 'E:\Example\';

output_file=['Data_Example'] ;

for iResistor = 1:length(resistance_sweep)
    % resistance of the oscilloscope
    if iResistor ==1
        Rosc=1;
    elseif iResistor==2
        Rosc=2.7;
    else
        Rosc=10;
    end

    file_location=[file_path];
    data_file = ['tek00' num2str(iResistor,'%.2dCH1.csv')];
    input_name = [file_location data_file];
    data = dlmread(input_name,',',22,0);

    Rvar= resistance_sweep(iResistor); %resistance value in
ohms

    %Time and voltage recording
    time = data(:,1);                   %seconds
    voltage = data(:,2);                %volts
    voltage =voltage-mean(voltage);     %center data around
zero
    raw_voltage(:,iResistor)=voltage;   %all raw voltage
data

    %Sample frequency claculation
    deltaT= diff(time);                 %sample freq
    DeltaT = mean(deltaT);
    fs=1/DeltaT;
    N=2^nextpow2(length(time));         %N points (2^n) for
the FFT

    %FFT and power spectrum calculation
    dt=1/fs;                            %time between
samples
    range=(N/2);                        %range for the
spectral plot
```

```
    f=fs*(0:range-1)/N;                     %frequency axis
(starts at 0)

    Y=fft(voltage);                         %FFT using amount
of data points recorded
    Pyy=Y.*conj(Y)/N;                       %Calculate the
Power spectrum

    %   PLOT the power spectrum of each data series
%         figure(1)
%         subplot(2,1,1)
%         plot(time,Y)
%         title('FFT')
%         xlabel('time (s)')
%         ylabel('Amplitude (V)')
%
%         hold on
%
%         subplot(2,1,2)
%         plot(f',Pyy(1:range))
%         title('Power Spectrum');
%         xlabel('Frequency (Hz)')
%         ylabel('V^2')
%
%         hold on

    %filter
    [b,a] = butter(5,2*fc/fs); % (Nth order, cutoff
frequency)how to determine cutoff freq
    Vosc = filtfilt (b,a,voltage);

    % Second FFT and power spectrum calculation AFTER
lowpass filter

%         figure(2)
%         Y=fft(Vosc);         % FFT
%         Pyy=Y.*conj(Y)/N;    % Calculate the Power
spectrum
%
%         subplot(2,1,1)
%         plot(time,Y)
%         title('FFT')
%         xlabel('time (s)')
%         ylabel('Amplitude (V)')
```

```
%
%         hold on
%
%         subplot(2,1,2)
%         plot(f',Pyy(1:range))
%         title('Power Spectrum');
%         axis ([0 100 0 .005]);
%         xlabel('Frequency (Hz)')
%         ylabel('V^2')
%
%         hold on

 % Variable calculations for voltage and power
    Vosc = Vosc*(1/sqrt(2));
% convert to RMS voltage
    Vout = Vosc.*(1+(Rvar/Rosc));
% scale voltage by the applied resistance - find voltage
produced by the speciman
    Vamp = (max(Vout) - (min(Vout)))/2;
% peak-to-peak voltage (amplitude)
    P = Vout.^2./(Rvar+Rosc);
% instantaneous power
    Pavg = trapz(time,P) * 1/(max(time) - min(time));
% average power
    Pmax = Vamp.^2./(Rvar+Rosc);
% peak power per cycle
    Pmaxu = Pmax*(10^6);

%% Store data to output

output(iResistor,:)={Rvar+Rosc, Vamp, Pavg, Pmaxu};


end

%% Output to an excel sheet for later analysis
output_header = {'Resistance (ohm)' 'P-P Voltage (V)' 'Pavg
(W)' 'Pmax (W)'};

output = [output_header; output];

   xlswrite([output_file '.xls'], output_header,1,'A1')
```

```
   xlswrite([output_file
'.xls'],output(2:length(resistance_sweep)+1,:),'Sheet1','A2
')


disp('Done')
```